MCB
Journals.ASM.org

Dynamic, Sex-Differential STAT5 and BCL6 Binding to Sex-Biased, Growth Hormone-Regulated Genes in Adult Mouse Liver

Yijing Zhang, Ekaterina V. Laz, and David J. Waxman

Division of Cell and Molecular Biology, Department of Biology, Boston University, Boston, Massachusetts, USA

Sex-dependent pituitary growth hormone (GH) secretory patterns determine the sex-biased expression of >1,000 genes in mouse and rat liver, affecting lipid and drug metabolism, inflammation, and disease. A fundamental biological question is how robust differential expression can be achieved for hundreds of sex-biased genes simply based on the GH input signal pattern: pulsatile GH stimulation in males versus near-continuous GH exposure in females. STAT5 is an essential transcriptional mediator of the sex-dependent effects of GH in the liver, but the mechanisms that underlie its sex-dependent actions are obscure. Here we elucidate the dynamic, sex-dependent binding of STAT5 and the GH/STAT5-regulated repressor BCL6 to mouse liver chromatin genome wide, revealing a counteractive interplay between these two regulators of sex differences in liver gene expression. Our findings establish a close correlation between sex-dependent STAT5 binding and sex-biased target gene expression. Moreover, sex-dependent STAT5 binding correlated positively with sex-biased DNase hypersensitivity and H3-K4me1 and H3-K4me3 (activating) marks, correlated negatively with sex-biased H3-K27me3 (repressive) marks, and was associated with sex-differentially enriched motifs for HNF6/CDP factors. Importantly, BCL6 binding was preferentially associated with repression of female-biased STAT5 targets in male liver. Furthermore, BCL6 and STAT5 common targets but not BCL6 unique targets showed strong enrichment for lipid and drug metabolism. These findings provide a comprehensive, genome-wide view of the mechanisms whereby these two GH-regulated transcription factors establish and maintain sex differences affecting liver physiology and disease. The approaches used here to characterize sex-dependent STAT5 and BCL6 binding can be applied to other condition-specific regulatory factors and binding sites and their interplay with cooperative chromatin binding factors.

Sex differences characterize the expression of more than 1,000 genes in mouse, rat, and human liver, affecting a wide range of biological processes, including steroid and lipid metabolism, inflammation, and diseased states (11, 55, 62, 67, 69). Sex differences in pharmacokinetics and pharmacodynamics have long been recognized and are in part a consequence of the sex-biased expression of cytochrome P450 (CYP) and other drug-metabolizing enzymes (19, 50, 52, 63, 68). Sex differences in human liver gene expression are widespread (69) and may contribute to sex differences in cardiovascular disease risk (69), fatty liver disease (1), and hepatocellular carcinoma (2, 58).

Growth hormone (GH), in particular its sex-dependent pituitary secretory pattern, is the major hormonal determinant of liver sex differences (38, 44, 63). In rats and mice, GH is secreted by the pituitary gland in a highly pulsatile manner in males, while in females GH secretion is more frequent, such that there is no prolonged GH-free interval between plasma hormone pulses (29, 54, 66). Ablation of circulating GH by hypophysectomy abolishes liver sex differences globally (61, 62), and exogenous GH pulses restore male-biased gene expression (27, 64). Continuous GH infusion in male mice mimics the female GH secretory pattern and induces female-biased genes while repressing male-biased gene expression in the liver (27). While large numbers of sex-dependent, plasma GH pattern-dependent genes have been identified, little is known about the molecular mechanisms whereby these genes respond robustly to their sex-differentiated hormonal input signals.

The transcription factor STAT5 (25) plays a prominent role in the transcriptional responses to GH, and it has been implicated in the sex-dependent effects of GH on liver gene expression. Liver STAT5 activity cycles in a dynamic, pulsatile manner in direct response to each sequential plasma GH pulse in male rat liver, whereas in female rat liver, STAT5 activity persists at a low level in response to the more frequent (near-continuous) stimulation by circulating GH (10, 65). STAT5b, in particular, is required to maintain the expression of ~90% of male-biased genes and for repression of a subset (~60%) of female-biased genes in male mouse liver, as has been shown in mouse knockout models (11, 26). However, it is unclear whether the sex-biased, STAT5-dependent genes identified are direct targets of STAT5 or whether their dysregulation in STAT5-deficient mice is a secondary response. It is also unclear why some direct STAT5 target genes, such as *Igf1* (8, 13, 36), do not show significant sex-biased expression.

Global gene expression analysis has identified many genes that respond to GH rapidly, several of which are known to be direct targets of STAT5 (60–62). These early GH response genes include several transcription factors that show sex-biased expression. One such factor is the transcriptional repressor BCL6 (5, 53), which shows male-biased expression in liver and is downregulated by the female plasma GH profile (43). BCL6 can modulate transcriptional responses to cytokines and other factors by binding to STAT response elements, enabling it to regulate a wide range of biological processes, including proliferation, differentiation, and apop-

Received 20 September 2011 **Returned for modification** 24 October 2011
Accepted 7 December 2011
Published ahead of print 12 December 2011
Address correspondence to David J. Waxman, djw@bu.edu.
Supplemental material for this article may be found at http://mcb.asm.org/.

doi:10.1128/MCB.06312-11

tosis (15, 16, 23, 24, 40). STAT5 and BCL6 have opposing effects on the transcriptional regulation of several GH response genes (6, 7, 43), suggesting that BCL6 might modulate the sex-biased effects of STAT5 on liver gene expression (43). Other transcription factors implicated in GH-dependent, sex-differential liver gene expression include the liver-enriched factors HNF4A and HNF6/Onecut1 (4, 14, 28, 33, 46) and the homeobox CDP family member CUX2 (CUTL2) (35). However, it is not known whether these factors cooperate with STAT5 to regulate liver sex differences.

Here, we identify STAT5 and BCL6 binding sites genome-wide in male and female mouse liver during both the peak and trough periods of plasma GH-activated STAT5, and we elucidate the interplay between these two factors in the regulation of sex-biased liver gene expression. Quantitative sex differences in STAT5 binding are determined for thousands of STAT5 binding sites and are shown to correlate well with sex-biased expression of STAT5 target genes. The sex-differential binding of STAT5 is also shown to be highly correlated with several sex-dependent epigenetic modifications and sex-differentially enriched motif families, the most prominent of which is HNF6/CDP. In addition, BCL6 binding sites that overlap with STAT5 binding sites are found to be preferentially associated with repression of female-biased genes in male liver. Finally, we identify lipid and cytochrome P450 metabolism among the top functional categories enriched in STAT5 and BCL6 common target genes, highlighting the importance of BCL6 in modulating these GH/STAT5-regulated metabolic processes. This comprehensive analysis of sex-dependent binding of two key GH-regulated transcription factors and their relationship to sex-dependent chromatin modifications provide important new insights into the mechanisms that control sex differences affecting hepatic lipid metabolism and other physiological and pathophysiological processes.

MATERIALS AND METHODS

Nucleus isolation, cross-linking, and DNA fragmentation. All animal protocols were approved by the Boston University Institutional Animal Care and Use Committee. Male and female CD-1 mice (Charles River Laboratories), 7 to 8 weeks old, were killed and their livers were extracted. Where indicated, mice were treated with recombinant rat GH (Protein Laboratories Rehovot, Ltd., Rehovot, Israel) by continuous infusion at 20 ng/g of body weight/h for 7 days using an Alzet osmotic minipump (model 1007D; Durect Corp., Cupertino, CA) (27). All mice were killed during the daytime. A portion of each liver was removed, snap-frozen in liquid nitrogen, and stored at −80°C followed by electrophoretic mobility shift analysis (EMSA) (see below) to determine the STAT5 DNA binding activity status of each liver sample. Nuclei were isolated from the remainder of each individual liver as described previously (22), with modifications. Briefly, approximately 80 to 90% of a mouse liver was homogenized in 8 ml of homogenization buffer (10 mM HEPES [pH 7.9], 25 mM KCl, 2 M sucrose, 0.15 mM spermine, 0.5 mM spermidine, 1 mM EDTA, 10% glycerol, and Complete protease inhibitor cocktail [1 tablet/25 ml; Santa Cruz Biotechnology]) and phosphatase inhibitors (either PhosSTOP phosphatase inhibitor cocktail [1 tablet/10 ml; Roche] or 10 mM sodium fluoride, 1 mM sodium orthovanadate). Each liver homogenate was layered over a 3-ml cushion of the same buffer and centrifuged for 30 min at 25,000 rpm at 4°C in an SW41 rotor. The pelleted nuclei were resuspended in 2.5 ml buffer containing 10 mM HEPES (pH 7.6), 25 mM KCl, 0.34 mM sucrose, 0.15 mM 2-mercaptoethanol, and 2 mM $MgCl_2$. Formaldehyde was added to a final concentration of 1%, and the samples were incubated with shaking for 9 min at 30°C. Following the addition of glycine to a final concentration of 0.125 M, the samples were incubated for 5 min at room temperature and then layered over a 3-ml cushion of the homogenization buffer in an SW41 rotor centrifuge tube. The tubes were centrifuged for 25 min at 25,000 rpm at 4°C in an SW41 rotor. The cross-linked nuclei were stored at −80°C. Individual nuclear pellets were resuspended in 2.4 ml of radioimmunoprecipitation assay (RIPA) buffer (50 mM Tris-HCl [pH 8.1], 150 mM NaCl, 1% IGEPAL CA-630, 0.5% sodium deoxycholate) containing 0.5% SDS and Complete protease inhibitor cocktail (1 tablet/50 ml) and then sonicated in 15-ml polystyrene tubes for 25 to 45 cycles (30 s on, 30 s off) at 4 to 10°C using a Bioruptor sonicator (Diagenode, Inc., Denville, NJ) at the high setting. Sonicated samples were centrifuged for 5 min at a maximum speed in a microcentrifuge at 4°C, and the chromatin supernatants were snap-frozen in liquid nitrogen and stored at −80°C. The majority of DNA fragments ranged from 100 to 400 bp, with some fragments ~800 bp long, as determined by agarose gel electrophoresis.

ChIP. Chromatin immunoprecipitation (ChIP) was carried out using STAT5 antibody C-17 (sc-835X, lot E0509), BCL6 antibody N-3 (sc-858X, lot J1003), and normal rabbit IgG (sc-2027, lot C0411), all from Santa Cruz Biotechnology, Inc., and methylated histone H3 antibodies K27me3 (ab6002), H3-K9me3 (ab8898), H3-K4me3 (ab8580), and H3-K4me1 (ab8895), all from Abcam, Inc. All steps were performed at 4°C, unless indicated otherwise. Sonicated cross-linked chromatin in RIPA buffer containing 0.5% SDS (typically 150 to 300 μg DNA/ml) was diluted with RIPA buffer containing Complete protease inhibitor cocktail to reduce the final SDS concentration to 0.1% and then further diluted with RIPA buffer containing 0.1% SDS and Complete protease inhibitor cocktail to equalize the DNA concentration across all samples to be immunoprecipitated with a given antibody. A 50-μl aliquot was removed from each sample and set aside as input control. Protein A-Dynabeads (Invitrogen) were preincubated overnight in PBS containing 0.5% bovine serum albumin (BSA) as follows: 40 μl Dynabeads plus 8 μg antibody to STAT5, BCL6, or normal rabbit IgG and 10 to 15 μl Dynabeads plus 1.2 to 3 μg antibody to methylated histone H3. The antibody-preincubated protein A-Dynabeads were then washed 3 times in PBS containing 0.5% BSA and added to the diluted sonicated chromatin: 100 μg sonicated chromatin DNA was used for STAT5, BCL6, and normal rabbit IgG (control) ChIP, and 15 μg sonicated chromatin DNA was used for methylated histone H3 ChIP. The samples were incubated overnight at 4°C. The beads were then washed twice with RIPA buffer containing 0.1% SDS, three times with RIPA buffer containing 0.1% SDS and 0.5 M NaCl, and once with TE buffer (10 mM Tris-HCl [pH 8.1], 1 mM EDTA) (1 ml/sample/wash), all at 4°C. The Dynabeads were incubated in elution buffer (50 mM Tris-HCl [pH 8.0], 10 mM EDTA, 1% SDS; 125 μl per 40 μl of beads) for 30 min at 65°C with periodic vortexing, and the supernatants were collected. The supernatants were incubated for 6 h at 65°C in the presence of 0.2 M NaCl to reverse cross-linking, followed by successive treatments with 0.12 mg/ml RNase A (Novagen, Gibbstown, NJ) for 30 min at 37°C and 0.39 mg/ml proteinase K for 2 h at 56°C. Extraction of DNA was performed with a QIAquick gel extraction kit (Qiagen) using the manufacturer's protocol. DNA concentrations were determined using a Quant-iT double-stranded DNA HS assay kit (Invitrogen). DNA samples (either undiluted or diluted up to 10 times in water) were analyzed by quantitative PCR (qPCR) to interrogate select genomic binding sites and then submitted for library preparation and ChIP-Seq analysis (see below). ChIP input control samples (50 μl) were incubated for 6 h at 65°C in the presence of 0.2 M NaCl to reverse cross-linking, followed by successive treatments with 5 μg of RNase A for 30 min at 37°C and with 20 μg of proteinase K for 2 h at 56°C. DNA was extracted with phenol-chloroform-isoamyl alcohol (25:24:1) and precipitated overnight at −20°C with ethanol in the presence of 15 μg glycogen (Ambion, Austin, TX). The pellets were washed with 95% ethanol, dissolved in 50 μl of water, and stored at −20°C. For qPCR analysis, the input samples were diluted 50-fold in water containing 50 μg/ml yeast RNA (Ambion) and assayed as described previously (36) using 1 μl of DNA template per assay.

Preparation of liver homogenates and EMSA. Liver homogenates were assayed for STAT5 DNA binding activity by EMSA as described below; individual livers were subsequently selected for STAT5 ChIP-Seq analysis based on their STAT5 EMSA activity profiles. All steps were performed as described earlier for rat liver (36). Briefly, liver homogenates (30 μg) were mixed with 2 μl of 7.5× EMSA buffer (75 mM Tris-HCl [pH 7.5], 365 mM NaCl, 30% glycerol, 7.5 mM $MgCl_2$, 3.75 mM EDTA, and 3.75 mM dithiothreitol) and 1 μl of a 2-μg/μl poly(dI-dC) acid solution, and the volume of each mixture was adjusted to 12.5 μl with water. Double-stranded DNA probe derived from the rat β-casein (*Csn2*) promoter (sense-strand sequence, 5′-GGACTTCTTGGAATTAAGGGA-3′) was labeled on one strand with [γ-^{32}P]ATP using T4 polynucleotide kinase and then added (2.5 μl per sample) to give a final concentration of 0.25 nM. Samples were incubated for 20 min at room temperature and then 10 min on ice, followed by electrophoresis on a 5.5% nondenaturing polyacrylamide gel in 0.5× Tris-borate-EDTA buffer. Gels were exposed to phosphor screens, followed by analysis on a Typhoon Trio variable-mode imager (GE Healthcare). Verification of liver STAT5 EMSA complexes by competition with excess unlabeled probe and by supershifting with anti-STAT5 antibody was reported previously (9, 36).

High-throughput sequencing. DNA isolated by ChIP was prepared for sequencing using a SPRI-TE nucleic acid extractor (Beckman Coulter Genomics, Danvers, MA) followed by PCR enrichment with barcoding. The SPRI-TE instrument automates end repair, A addition, Illumina adapter ligation, and size selection (200 to 400 nucleotides [nt]). Sample preparation and 35-nt, single end read sequencing on an Illumina GAII instrument (San Diego, CA) were carried out at the BioMicro Center at MIT (Cambridge, MA). Male (M) and female (F) STAT5 ChIP samples are designated MH and FH to indicate that ChIP was carried out using livers with high STAT5 EMSA activity (H) at the time the mice were killed (STAT5-MH and STAT5-FH); ML and FL indicate ChIP was carried out using with livers with low STAT5 EMSA activity (STAT5-ML and STAT5-FL). Male and female BCL6 ChIP samples were designated BCL6-M and BCL6-F, respectively.

ChIP-Seq data analysis. MACS software (70) with default parameters was used for peak calling, with peaks defined as those genomic regions showing significant enrichment of sequence reads at $P < 10E-25$ (MACS score, 250). For peak identification, STAT5-high and STAT5-low samples, as well as BCL6-male samples, were normalized to IgG controls, as implemented in MACS. Initial analysis showed that biological replicates of STAT5-high liver samples showed high correlations between individual samples for males and separately for STAT5-high females (see Fig. S1A in the supplemental material), allowing us to carry out MACS analysis using combined data sets comprised of data for individual livers in each group of the same sex and STAT5 activity status. To quantitatively compare STAT5 ChIP-Seq data sets between male and female livers, we first merged the STAT5-MH and STAT5-FH peak sets, resulting in a list of 15,094 merged peaks. Next, we determined which of the 15,094 merged peaks were common to the STAT5-MH and STAT5-FH peak sets. The number of sequence reads from each sample in each of the common peaks was then used to rescale the data by a linear transformation, such that, overall, the common peaks had a mean male to female ratio of 1.0. This normalization method, called MAnorm, removes the global dependence of the M value ($\log_2$ sequence read ratio) on the A value ($\log_2$ sequence read density) for the set of STAT5 common peaks. STAT5 peaks with M values of >1 were defined as male-enriched peaks, and those with M value of <-1 were defined as female-enriched peaks (i.e., peaks with a >2-fold sex difference in normalized sequence reads).

Enrichment *P* values were calculated using Fisher exact test. When comparing STAT5 and BCL6 peak sets, the overlap between the peak sets being compared was calculated after trimming the peaks to a total width of 600 nt centered at the peak summit. ChIP-Seq peaks were compared to chromatin mark data sets (57) and to the set of 72,862 global mouse liver DNase hypersensitivity (DHS) sites identified previously (39), which correspond to open chromatin regions. For both the male and female DHS and H3-K27me3 data sets, sequence reads in the liver samples comprising each set were rescaled based on the total number of mapped sequence reads, to facilitate comparisons between male and female liver samples. For other histone marks (H3-K4me1, H3-K4me3, and H3-K9me3), the number of reads was rescaled based on the number of reads in male and female common peaks for each mark. To plot the sequence read distribution around each peak summit (see, for example, Fig. S3A to F in the supplemental material), the total number of reads in each 100-bp interval was summed for all peaks in a given peak set, and the results were plotted in 1-bp-step sizes after normalization based on the number of peaks in each set. PeakSplitter software (http://www.ebi.ac.uk/bertone/software/) was used to subdivide the broad, complex peaks associated with each STAT5 and BCL6 peak set into individual binding sites and to identify their peak summits (see Table S4 in the supplemental material).

STAT5 and BCL6 peak targets. For each ChIP-Seq peak, the peak target was defined as the nearest gene whose gene body was located within 10 kb upstream or 10 kb downstream of the peak region. Male-enriched STAT5 targets were defined as genes targeted by one or more male-enriched STAT5 peaks but not by a female-enriched STAT5 peak, independent of whether the gene was also the target of a STAT5 male-female common peak. A corresponding definition was used for female-enriched STAT5 targets. All STAT5 target genes that were not associated with a male-enriched or female-enriched STAT5 peak or that were associated with both a male-enriched and a female-enriched STAT5 peak were defined as a STAT5 common target.

***De novo* motif discovery and motif enrichment analysis.** *De novo* motif discovery was carried out using Flexmodule motif in the CisGenome package (30) with default parameters. In some cases, peak coordinates were trimmed around the peak summit as specified in the text. Motif enrichment analysis was carried out for each ChIP-Seq data set by using the subset of peaks that overlapped with the set of DHS sites determined previously (39). The DHS-overlapping ChIP-Seq peaks likely represent the most reliable set of transcription factor binding sites, based on the following: (i) 70 to 98% of the peaks in each STAT5 and BCL6 ChIP-Seq data set overlap with a liver DHS site (see Table 1), and (ii) we observed a similarly high percentage of overlap between factor binding sites and liver DHS sites in our analysis of six other transcription factors (39). Motif enrichment was calculated as follows: first, Motifmap_matrixscan_genome in CisGenome (30) was used to scan all peaks that overlapped DHS sites (200 bp upstream and 200 bp downstream of the DHS center) for matches to a set of 97 motif matrices (numbered 0 to 96) derived from the TRANSFAC and JASPAR databases and described previously (41), replacing the STAT5 motif with the *de novo*-discovered STAT5 motif (classes I to III) identified in this study, and adding one BCL6 unique motif (class VII) (see Fig. 6B). Next, for each motif, we calculated the ratio of the motif occurrence in the subset of each STAT5/BCL6 peak list that overlapped a DHS site (recorded as ratio 1) and also the motif occurrence in all DHS sites that did not overlap with a STAT5 peak or a BCL6 peak (recorded as ratio 2); the enrichment of the motif in each peak list equals ratio 1 divided by ratio 2. Motifs enriched with an enrichment score (ES) of >1.7 and Fisher exact test *P* value of $<1E-10$ (unless otherwise stated) in at least one of the seven peak lists comprising STAT5 and BCL6 classes I to VII (see Fig. 6A) were clustered and are presented in a heat map (see Fig. 8A).

Gene expression data. Gene expression data for both intact and hypophysectomized adult male and female ICR mice were obtained from earlier studies (27, 61) based on a microarray significance cutoff of $P < 0.001$ to identify genes showing sex-specific expression (2,876 sex-biased RefSeq genes) and to identify genes induced or repressed by hypophysectomy. In other cases, a significance threshold for the male-female |fold change| of >1.5 combined with a *P* value of <0.05 was applied, yielding 2,282 sex-biased RefSeq genes. Y chromosome genes were excluded from the analysis.

GO term and gene set enrichment analysis. A total of 8,332 gene ontology (GO) terms and associated gene lists were downloaded (http:

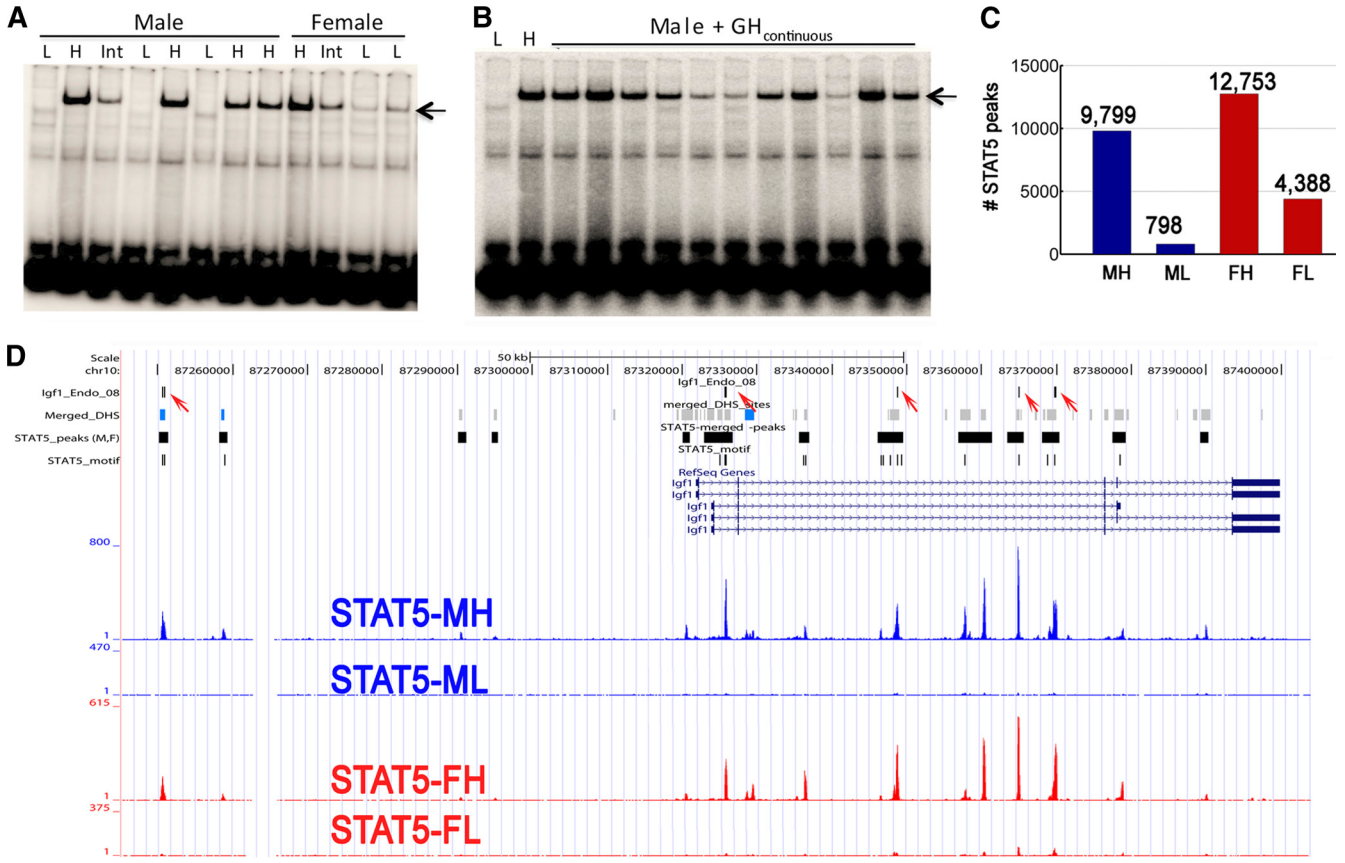

FIG 1 Dynamic nature of STAT5 binding in male versus female mouse liver. (A) EMSA gel showing STAT5 DNA binding activity status of 8 individual male and 4 individual female mouse livers. STAT5 activity was high (H), low (L), or intermediate (Int) in individual livers. STAT5 activity was substantially above background in low-activity female livers but was undetectable in low-activity male livers. The arrow at the right identifies STAT5 EMSA complex. (B) Continuous infusion of male mice with GH for 7 days abolished the pulsatile (intermittent) nature of liver STAT5 activity seen in untreated males, as indicated by the absence of STAT5 activity-free male livers in the set of 12 individuals shown and in other sets of male livers (data not shown). Typically, 30 to 60% of randomly selected untreated male livers show a STAT5-high or STAT5-intermediate EMSA profile. The two lanes on the left are from untreated males showing low and high STAT5 activity, as indicated. Arrow, STAT5 EMSA complex. (C) Number of STAT5 peaks identified by ChIP-Seq in each of the 4 indicated groups of livers, which differed by sex and by high versus low STAT5 activity status. Detailed peak lists are provided in Table S1 of the supplemental material. (D) UCSC Genome Browser view of the distribution of STAT5 reads around *Igf1*. The track with 5 red arrows indicates 5 STAT5 binding regions identified by ChIP-PCR (17). Other tracks mark liver DHS sites (39), STAT5 peaks in the merged STAT5 peak set (see Table S1F in the supplemental material), and occurrences of the *de novo*-discovered STAT5 motif identified in this study. The bottom four tracks show the STAT5 ChIP-Seq reads for the four indicated groups, displayed as wig files generated using MACS software with a sliding window average of 100 bp and a 20-bp step size. STAT5 tracks were normalized to the STAT5-MH sample (see Fig. S1E in the supplemental material).

//david.abcc.ncifcrf.gov/knowledgebase/DAVID_knowledgebase.html). For each of the gene sets comprising the STAT5 and BCL6 peak target classes I to VII (see Fig. 6B, below), the Fisher exact test was used to determine the enrichment *P* value of each GO term in the given gene list, compared to the occurrences of the GO term in all RefSeq genes. GO terms were considered enriched if they met the following criteria: ES $>$ 2.5, enrichment $P < 0.01$, and number of genes in the particular term $>$ 8. Enriched GO terms were hierarchically clustered with respect to ES. Gene set enrichment analysis was carried out to determine the significance of sex-specific STAT5 targets in sex-differentially expressed genes (http://www.broadinstitute.org/gsea/index.jsp) (56).

Accession numbers. Raw and mapped sequencing reads and bed files (listing MACS peaks with a score >50) for individual livers (see Fig. S1A in the supplemental material) are available in the GEO database (GSE31578; samples GSM784027 to GSM784045) and the Sequence Read Archive (SRA) database (SRP007992; samples SRX094449 to SRX094467). Liver DNase-seq data sets identifying DHS sites in male and female liver (39) are available under GEO accession no. GSE21777 (samples GSM542592 to GSM542601) and SRA accession no. SRP002445 (samples SRX020259 to SRX020268). Microarray gene expression data (61) are available under GEO accession no. GSE17644 (samples GSM440277 to GSM440298).

RESULTS

Plasma GH dependence of mouse liver STAT5 activity. STAT5 is repeatedly activated by each successive plasma GH pulse in male rat liver, whereas in female rat liver STAT5 activity persists at a low level in response to the more continuous stimulation by circulating GH (10, 65). Mouse liver also showed an overall pattern of intermittent pulses of STAT5 activity in males versus persistence of STAT5 activity in females; however, unlike rats, female mice routinely showed high peaks of STAT5 activity indistinguishable from those found in male liver (Fig. 1A). This species difference in liver STAT5 activity profiles suggests that a critical factor in the sex-differential effects of GH and STAT5 on liver gene expression is not the presence of high STAT5 activity in males versus low

TABLE 1 Peaks identified by STAT5 and BCL6 ChIP-Seq[a]

ChIP-seq peak set	No. of peaks	M-DHS				F-DHS		
		% overlap with DHS	No. overlapping an M-DHS	ES	*P* value	No. overlapping an F-DHS	ES	*P* value
STAT5-MH enriched	1,765	70	569	14.26	<1E−100	1	0.05	1E+00
STAT5-FH enriched	1,791	77	22	0.49	1E+00	161	7.86	7E−94
STAT5-MH and -FH common	11,538	92	589	1.70	3E−44	74	0.47	1E+00
STAT5-ML	798	98	35	1.37	3E−02	2	0.17	1E+00
STAT5-FL	4,388	99	42	0.30	1E+00	117	1.80	2E−10
BCL6-M	6,432	93	311	1.60	4E−18	87	0.98	5E−01
BCL6-F	909	94	14	0.50	1E+00	28	2.19	8E−05

[a] STAT5 peaks were identified in STAT5 high-activity livers (STAT5-MH and STAT5-FH) and in STAT5 low-activity livers (STAT5-ML and STAT5-FL) from male (M) and female (F) mice. The STAT5-MH and STAT5-FH peaks were subdivided into three groups: male-enriched and female-enriched peaks and STAT5 male and female common peaks, as illustrated in the top (left) Venn diagram of Fig. 6A and as shown in the first 3 lines of this table. For each set of ChIP-Seq peaks, the number of peaks that overlapped with a liver DHS site (39) is shown as a percentage. Also shown is the number of ChIP-Seq peaks in each set that overlapped with either a male-specific or female-specific mouse liver DHS site (M-DHS and F-DHS), identified previously (39). The fold enrichment of each set of STAT5 and BCL6 ChIP-Seq peaks at male DHS sites or female DHS sites is indicated by an ES and by a Fisher exact test *P* value. Male-enriched STAT5 peaks showed strong enrichment at male DHS sites (ES, 14.26), while female-enriched STAT5 peaks showed strong enrichment at female DHS sites (ES, 7.86). Further details are provided in Table S1A of the supplemental material.

STAT5 activity in females, which is seen in rat liver (10, 65) but not mouse liver (Fig. 1A); rather, the key sex difference may be the absence in female liver of a sustained time interval when STAT5 activity is shut off, which is a characteristic of female rats (9) and also female mice (Fig. 1A). To test this hypothesis, male mice were given a continuous, 7-day infusion of GH. This treatment feminizes liver gene expression (27) and liver chromatin structure (39), and as shown here (Fig. 1B), it abolishes the intermittent STAT5 activity-off time periods that characterize untreated males (Fig. 1A, male lanes marked L) without downregulating STAT5 activity. We conclude that intermittent (male) versus persistent (female) STAT5 signaling is a critical feature of GH-regulated liver sex differences.

Dynamic nature of global STAT5 binding deduced from ChIP-Seq analysis. ChIP-Seq was carried out using STAT5 antibody and sonicated, cross-linked chromatin prepared from livers excised from individual untreated male and female mice killed at a peak of STAT5 activity or during the interpulse interval, when STAT5 activity is either low (females) or undetectable (males), as determined by EMSA. Many more STAT5 peaks were identified in STAT5 high-activity male and female livers (STAT5-MH and STAT5-FH peaks, respectively) than STAT5 low-activity livers (STAT5-ML and STAT5-FL peaks) (Fig. 1C; Table 1), consistent with the EMSA profiles shown in Fig. 1A. Full details on the peaks identified, including significance scores, genomic coordinates, overlap with liver DHS sites (39), presence of motifs for STAT5 and other factors, and target genes of each peak and their sex-dependent regulation, are provided in Table S1 of the supplemental material. ChIP-Seq results were verified for select STAT5 binding sites by qPCR (see Fig. S1B in the supplemental material). All four STAT5 peak sets (Fig. 1C) showed similar peak distributions in relation to gene annotations, with 6 to 9% of peaks found at promoters, 42 to 48% found in introns, and 39 to 45% found in intergenic regions (see Fig. S1D). 77% of the STAT5-MH peaks map to the same, or overlapping, genomic loci as STAT5-FH peaks, consistent with the strong overall correlation between these two ChIP-Seq peak sets (see Fig. S1F). Lower correlations were obtained for comparisons to STAT5-ML and STAT5-FL peaks (see Fig. S1G).

STAT5 targets, defined as genes that contain a STAT5 binding site within 10 kb of the gene body, showed enrichment (ES, 1.4; *P*, 1E−4) for genes that respond rapidly (within 30 min) to a pulse of GH (61). A total of 100 STAT5 targets were rapid GH response genes (see Table S2A in the supplemental material), including the well-characterized GH/STAT5-responsive genes *Igf1*, *Socs2*, and *Cish* (7, 8, 36, 60). In the case of *Igf1*, all 5 STAT5 binding sites identified by ChIP-PCR (17) showed strong peaks in both male and female STAT5 high-activity livers (Fig. 1D). Importantly, the STAT5-low livers showed very low sequence read densities at all STAT5 binding sites mapping to *Igf1* (Fig. 1D) and *Socs2* and *Cish* (see Fig. S1E in the supplemental material). This striking difference in the level of STAT5 binding between STAT5-high and STAT5-low livers indicates that STAT5 binds to these and thousands of other sites in a dynamic manner in response to each pulse of plasma GH stimulation.

STAT5 binding sites in STAT5-high versus STAT5-low livers. A substantial majority (80 to 83%) of the STAT5 binding sites (peaks) identified in STAT5-low livers were also bound by STAT5 in STAT5-high livers (Fig. 2A and B, Venn diagrams). Conceivably, these STAT5-high and STAT5-low liver "common peaks" may correspond to strong STAT5 binding sites, where DNA binding during the time of a plasma GH pulse (STAT5-high liver) persists after liver STAT5 activity is downregulated upon termination of a plasma GH pulse (STAT5-low liver). To test this hypothesis, we determined the overlap of STAT5-high peaks with STAT5-low peaks as a function of STAT5-high peak score, a general indicator of strength of binding activity. A steep slope is seen at the beginning of the curves followed by a slower decline with decreasing STAT5-high peak score (Fig. 2A and B), indicating that the STAT5 binding sites in STAT5-low livers tend to be strong binding sites. Consistently, the STAT5-high and STAT5-low common peaks have the highest number of sequence reads (see Fig. S2A to D in the supplemental material).

De novo motif discovery identified a motif very similar to the TRANSFAC STAT5B matrix in both male and female STAT5-high peak sets (Fig. 2C). This STAT5 motif showed highest enrichment in the summits of the set of 9,139 STAT5-MH unique peaks (as defined in Fig. 2A), with a lower enrichment seen in STAT5-MH and STAT5-ML common peaks and no motif enrichment detected around STAT5-ML unique peaks (Fig. 2D). The same pattern was seen with STAT5-FH compared to STAT5-FL peaks (Fig. 2E). Many STAT5 peaks, including some of the stron-

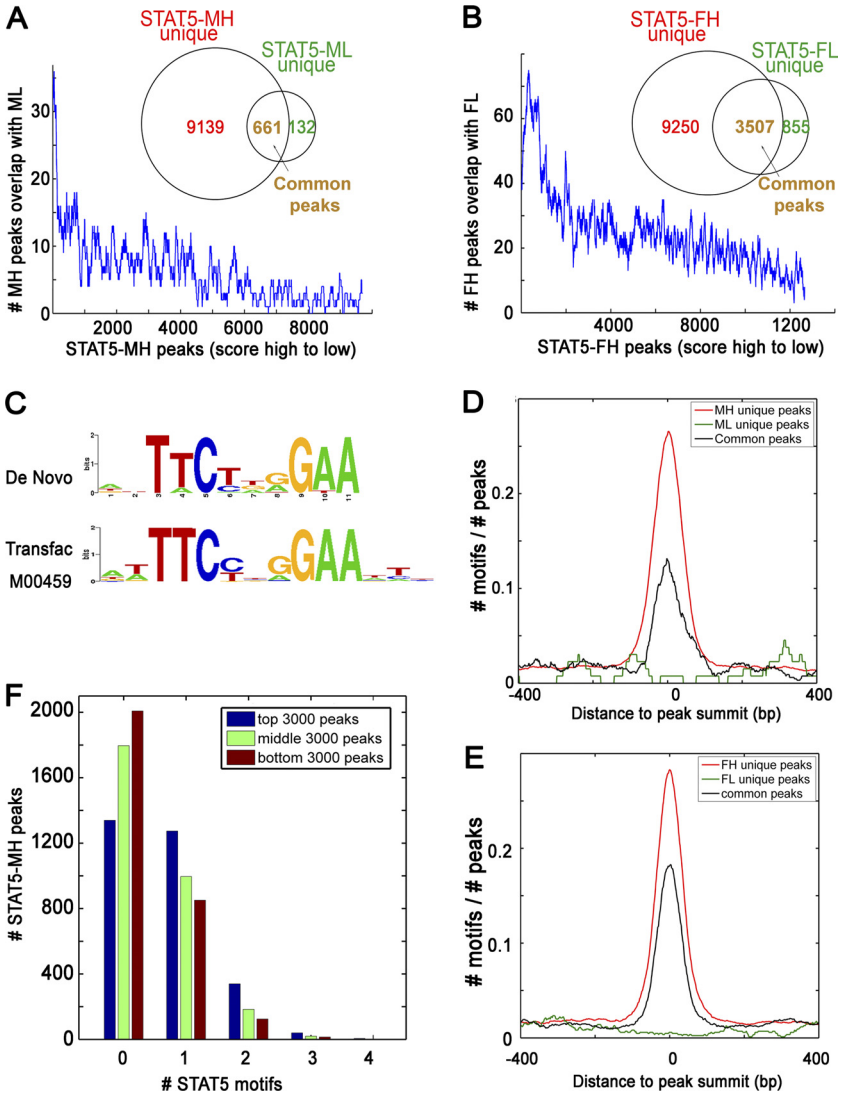

FIG 2 STAT5 binding sites and motifs in STAT5-high and STAT5-low livers. (A) Graph showing the number of STAT5-MH peaks (9,799 peaks ranked along the *x* axis by MACS peak score in descending order) that overlapped with STAT5-ML peaks in each consecutive set of 100 peaks, using a step size of 1 peak. (Inset) Venn diagram comparing the STAT5-MH and STAT5-ML peak sets, indicating the number of STAT5-MH peaks that were in common with the STAT5-ML peak set ("common peaks") and the number of peaks that were unique to each peak set. (B) Graph showing the number of STAT5-FH peaks that overlapped with STAT5-FL peaks in each consecutive set of 100 peaks (12,753 STAT5-FH peaks ranked along the *x* axis), analyzed as described for panel A. (Inset) Venn diagram comparing the STAT5-FH and STAT5-FL peak sets, indicating the number of STAT5-FH peaks that are in common with the STAT5-FL peak set (common peaks) and the number that are unique to each peak set. (C) Sequence logo representing the enriched STAT5 motif identified by *de novo* motif discovery applied to STAT5-MH peaks (top). This logo is almost identical with that discovered *de novo* from the STAT5-FH peak set (data not shown) and is very similar to the Transfac STAT5B matrix logo (bottom). (D) Distribution of the STAT5 motif around the summits of STAT5-MH unique and STAT5-ML unique peaks and in peaks common to both sets, as defined in the Venn diagram in panel A. (E) Corresponding distribution for the STAT5-FH unique and the STAT5-FL unique peaks and for the peaks common to both sets, as defined in the Venn diagram in panel B. Shown along the *y* axis is the total number of motifs in each consecutive window of 60 bp, with a step size of 1 bp, normalized to the total number of peaks in each sample. (F) High-quality STAT5 ChIP-Seq peaks have greater numbers of STAT5 motifs. Shown is the number of STAT5-MH peaks that contained 0, 1, 2, 3, or 4 occurrences of a STAT5 motif in each peak, determined for the three indicated subsets of STAT5-MH peaks and grouped based on the STAT5 ChIP-Seq MACS score. STAT5-FH peaks produced a very similar pattern (data not shown).

gest peaks, apparently do not contain STAT5 motifs (Fig. 2F). This observation, which is commonly seen in ChIP-Seq data sets (e.g., see Table 2 of reference 39), could reflect nonconsensus STAT5 sequences, or perhaps indirect STAT5 binding via other proteins present in the cross-linked chromatin complex. Fifty-five percent of the top STAT5-MH peaks (ranked by peak score) contained the *de novo* STAT5 motif, compared to ~40% in the middle and 33% in the bottom peak sets. For those STAT5-MH peaks that had a STAT5 motif, 23% of the top peaks contained two or more motifs, versus only 17% and 14% in the middle and bottom peak sets (Fig. 2F). Thus, strong STAT5 binding results when multiple STAT5 sites are in close proximity. Other motifs differentially enriched in STAT5-high versus STAT5-low peak sets are shown in Fig. S2E to F of the supplemental material.

Differential binding of STAT5 in male versus female livers. To identify sex differences in STAT5 binding, we quantitatively

compared the STAT5-MH and STAT5-FH peak sets after normalization based on the sequence reads in STAT5 common peaks (see Materials and Methods). Figure 3A presents the male-enriched STAT5 peaks (blue) and the female-enriched STAT5 peaks (red), graphed as the $\log_2$ male versus female sequence read ratio (M-value) versus the average $\log_2$ sequence read density (A-value). A 2-fold difference in normalized sequence read density was used as the cutoff to define sex-enriched STAT5 peaks (i.e., $|M| > 1$). Thus, we identified 1,765 male-enriched STAT5 peaks and 1,791 female-enriched STAT5 peaks, as well as 11,538 peaks not showing significant sex bias (male and female common peaks) (Fig. 3A and Table 1; see also Table S1F in the supplemental material). Stronger STAT5 binding was generally observed at the STAT5 common peaks than at the male-enriched or female-enriched peaks (higher A-value) (Fig. 3A; see also Fig. S3A and B in the supplemental material).

The STAT5 motifs obtained by *de novo* motif discovery were nearly identical for the male-enriched and female-enriched STAT5 peak sets. Moreover, these motifs were enriched in each peak set to a similar extent (Fig. 3B). This indicates that the sex-differential binding of STAT5 is not dictated by differences in the STAT5 motif but by other factors, such as epigenetic modifications and associated transcription factors. One such associated factor may be BCL6, as discussed below. Another factor may be from the HNF6/CDP family, as its motif showed significant enrichment in the male-enriched STAT5 peak set (ES, 2.6) but not in the female-enriched or STAT5 common peak sets. Importantly, the frequency of HNF6/CDP motifs showed a close association with the extent to which STAT5 binding was male enriched (M-value) (Fig. 3C, left). Other motifs enriched in STAT5-MH peaks compared with STAT5-FH peaks included those for HNF1, Pbx1, and Nkx2-5/HOXA4 (all ES, ~1.6). In addition, STAT5-FH peaks showed enrichment for motifs for EGR (ES, 2.1) and E2F1 (ES, 1.5) compared with STAT5-MH peaks.

Relationship between sex-differential STAT5 binding and epigenetic marks. Next, we investigated whether the observed sex differences in STAT5 binding are related to sex differences in liver chromatin accessibility, as determined by access to DNase digestion (DHS sites) (39), which is a characteristic of open chromatin structures. We also investigated the relationship to histone H3-K27me3 marks, which are generally associated with inactive, repressed genomic regions (42). Figure 3D shows a plot of the male to female ratio of DHS sequence reads, and also H3-K27me3 sequence reads, versus STAT5 peak sex specificity, ranked from male-enriched to female-enriched STAT5 peaks along the *x* axis; higher *y* axis values indicate greater chromatin opening (DHS sites) and more H3-K27me3 (repressive) marks in male versus female liver. Male-enriched STAT5 binding was seen to occur at genomic regions that were more open and depleted of H3-K27me3 marks in male liver, while female-enriched STAT5 binding occurred at regions more open and depleted of H3-K27me3 marks in female liver. This conclusion is supported by the very strong enrichment of male-enriched STAT5 binding sites at male-specific DHS sites (ES, 14.26) and of female-enriched STAT5 binding sites at female-specific DHS sites (ES, 7.86) (Table 1). Genomic regions associated with STAT5 peaks not showing significant sex differences (STAT5 common peaks) did not show sex differences in chromatin accessibility or H3-K27me3 marks (Fig. 3D, M values between 1 and −1). Further analysis revealed a positive association between male-enriched STAT5 sites and male-enriched marks for H3-K4me1 and H3-K4me3 (Fig. 3E, left), both generally associated with gene activation (3). A weaker association was seen between female-enriched STAT5 sites and female-enriched H3-K4me1 and H3-K4me3 marks (Fig. 3E, right). A weak negative association was seen between male-enriched STAT5 sites and male-enriched H3-K9me3, a repressive mark (Fig. 3E).

An interesting chromosome modification pattern around sex-specific STAT5 binding sites was seen when DHS and H3-K27me3 sequence reads around peak summits were plotted separately for male and female liver. In male liver, although sites represented by male-enriched STAT5 peaks had fewer H3-K27me3 reads than female-enriched STAT5 sites (see Fig. S3E in the supplemental material), they showed the same chromosome accessibility (DHS read density) as the female-enriched STAT5 sites (see Fig. S3C). In contrast, in female liver, sites represented by male-enriched STAT5 peaks were less accessible than the female-enriched STAT5 sites (see Fig. S3D), but the male-enriched STAT5 sites had only a moderately higher level of H3-K27me3 marks (see Fig. S3F). These findings support a role for sex-dependent epigenetic mechanisms in sex-biased STAT5 binding (Fig. 3F).

Sex-dependent STAT5 binding sites target sex-biased genes. Mapping of STAT5 peaks to nearby (within 10 kb) RefSeq genes identified 706 genes associated with one or more male-enriched STAT5 binding sites (male STAT5 targets) and 944 genes associated with female-enriched STAT5 binding sites (female STAT5 targets); the remaining genes, representing STAT5 common targets, were not uniquely associated with a sex-dependent STAT5 binding site (Fig. 4A). Next, we investigated the relationship between STAT5 targets and genes affected by hypophysectomy, which ablates circulating GH, the major regulator of liver STAT5 activity, and abolishes liver sex differences almost entirely (61). Male STAT5 targets are enriched in genes downregulated in male liver following hypophysectomy (ES, 2.3 to 2.5) (Fig. 4B). Female STAT5 targets showed an even greater enrichment in genes repressed by hypophysectomy in female liver but not male liver (ES, 3.7; $P = 2.3E-8$). STAT5 common targets are enriched in genes repressed by hypophysectomy in both sexes (ES, 2.0; $P = 0$) (Fig. 4B), consistent with GH-activated STAT5 stimulating expression of these genes in a sex-independent manner. STAT5 target genes that include at least one STAT5 peak containing a STAT5 motif showed highly significant enrichment for genes repressed by hypophysectomy compared to genes induced by hypophysectomy in both male and female liver, indicating the importance of a STAT5 motif for positive regulation by pituitary GH (Fig. 4C). In contrast, no differential effects on hypophysectomy-repressed versus hypophysectomy-induced genes were seen for those STAT5 target genes without a STAT5 motif associated with the STAT5 peak.

A substantial fraction (35%) of sex-biased genes were STAT5 target genes, with the percentage increasing to ~40% when genes within 50 to 90 kb of a STAT5 binding site were considered (Fig. 4D). Moreover, the sex bias of STAT5 binding often matched the sex specificity of gene expression, as shown for select sex-specific genes (Fig. 5; see also Fig. S1E in the supplemental material). Importantly, we observed a strong correlation between the presence of a sex-enriched STAT5 binding site and the extent of sex bias in target gene expression (Fig. 4E). Moreover, a substantially higher fraction of male-enriched STAT5 targets showed male-biased expression than female-enriched STAT5 targets (Fig. 4E, left, blue versus pink curve). An even greater fraction of female-enriched

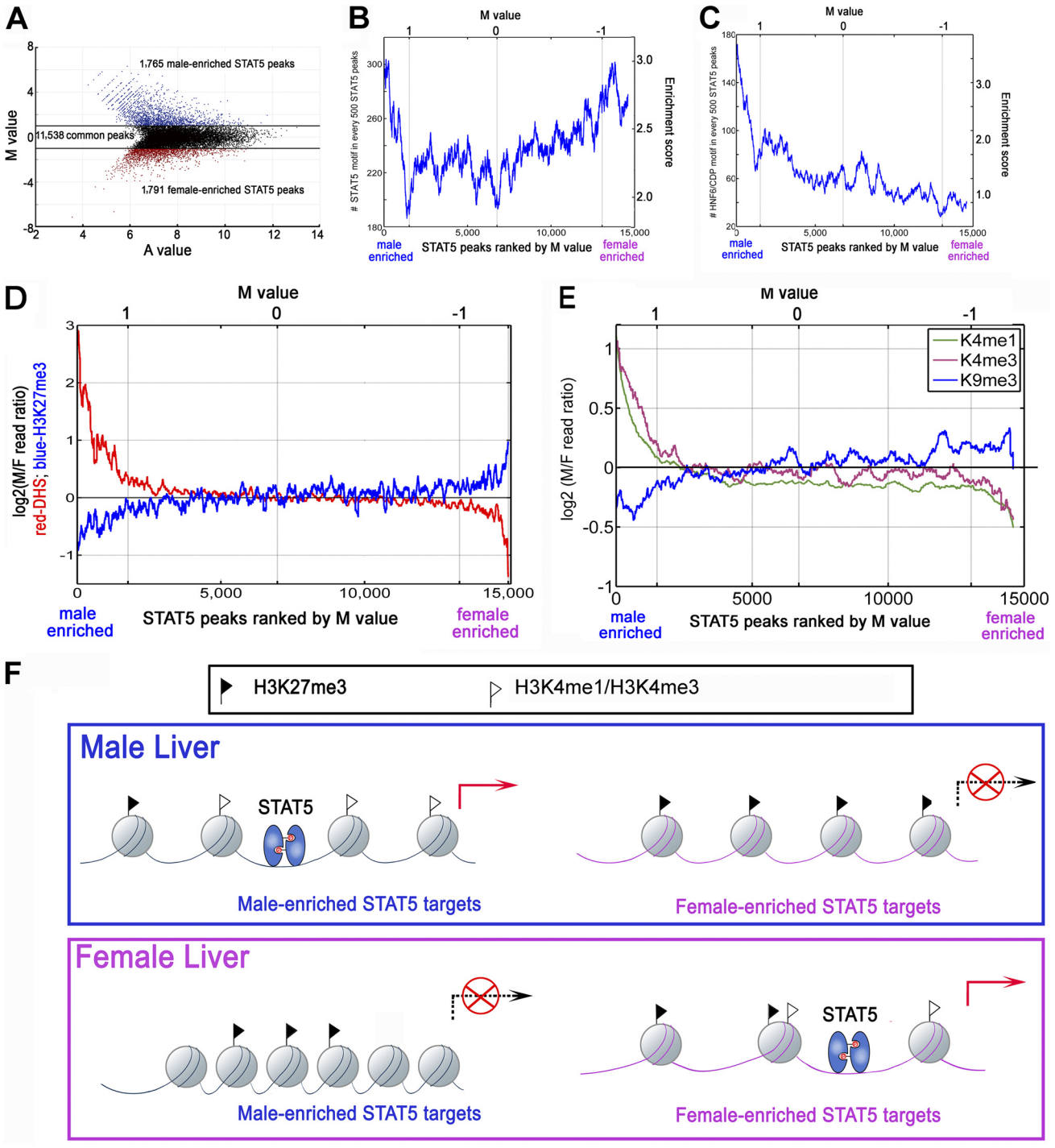

FIG 3 Male-enriched and female-enriched STAT5 peaks: association with HNF6/CDP motifs and epigenetic marks. (A) An M versus A plot of the number of STAT5-MH reads versus STAT5-FH reads in the set of 15,094 merged STAT5 peaks (see Table S1F in the supplemental material) after normalization using MAnorm (see Materials and Methods). Each peak is associated with an M-value and an A-value: $M = \log_2[(\text{number of STAT5-MH sequence reads})/(\text{number of STAT5-FH reads})$; $A = 0.5 \times [\log_2(\text{number of STAT5-MH reads}) + \log_2(\text{number of STAT5-FH reads})]$. Using a fold change of >2 as the cutoff (|M value|, >1; the pair of horizontal black lines), we identified 1,765 STAT5-MH-enriched peaks (blue dots), 1,791 STAT5-FH-enriched peaks (red dots), and 11,538 common peaks (black dots). The total number of STAT5 peaks (15,094) corresponded to the STAT5-MH and STAT5-FH merged peak set (see Materials and Methods). Full details for each peak are shown in Table S1F of the supplemental material. (B and C) Number of *de novo*-discovered STAT5 motifs (B) and HNF6/CDP family motifs (C) found in each consecutive set of 500 merged STAT5 peaks ranked according to the ratio of male to female STAT5 binding activity, i.e., high M-value (male-enriched STAT5 peaks) to low M-value (female-enriched STAT5 peaks). The M-value scale is shown along the top axis, the STAT5 peak rank is shown along the bottom axis, and the enrichment score is shown along the right axis. (D) Sex ratio of DHS site (red) and H3-K27me3 (blue) sequence reads ($\log_2$ scale) versus sex enrichment of the set of 15,094 merged STAT5 peaks ranked by M-value, as in panels B and C. (E) Sex ratio of H3-K4me1 (green), H3-K4me3 (purple), and H3-K9me3 (blue) sequence reads ($\log_2$ scale) versus sex enrichment of the set of 15,094 merged STAT5 peaks ranked by M-value. (F) Model depicting sex differences in chromatin accessibility, H3-K27me3 marks (black flags), and H3-K4me1 and H3-K4me3 marks (white flags) around sex-dependent STAT5 binding sites, based on the findings shown in panels D and E; see also Fig. S3D to F in the supplemental material. Sex-enriched STAT5 binding correlated positively with gene expression status (forward arrow), chromatin accessibility, and H3-K4me1 and H3-K4me3 marks and negatively with H3-K27me27 marks. However, female-enriched STAT5 binding sites in male liver showed more open chromatin than male-enriched STAT5 binding sites in female liver (compare Fig. S3C and D in the supplemental material), despite the somewhat higher level of H3-K27me3 marks at the female-enriched STAT5 binding sites (compare Fig. S3E with F in the supplemental material).

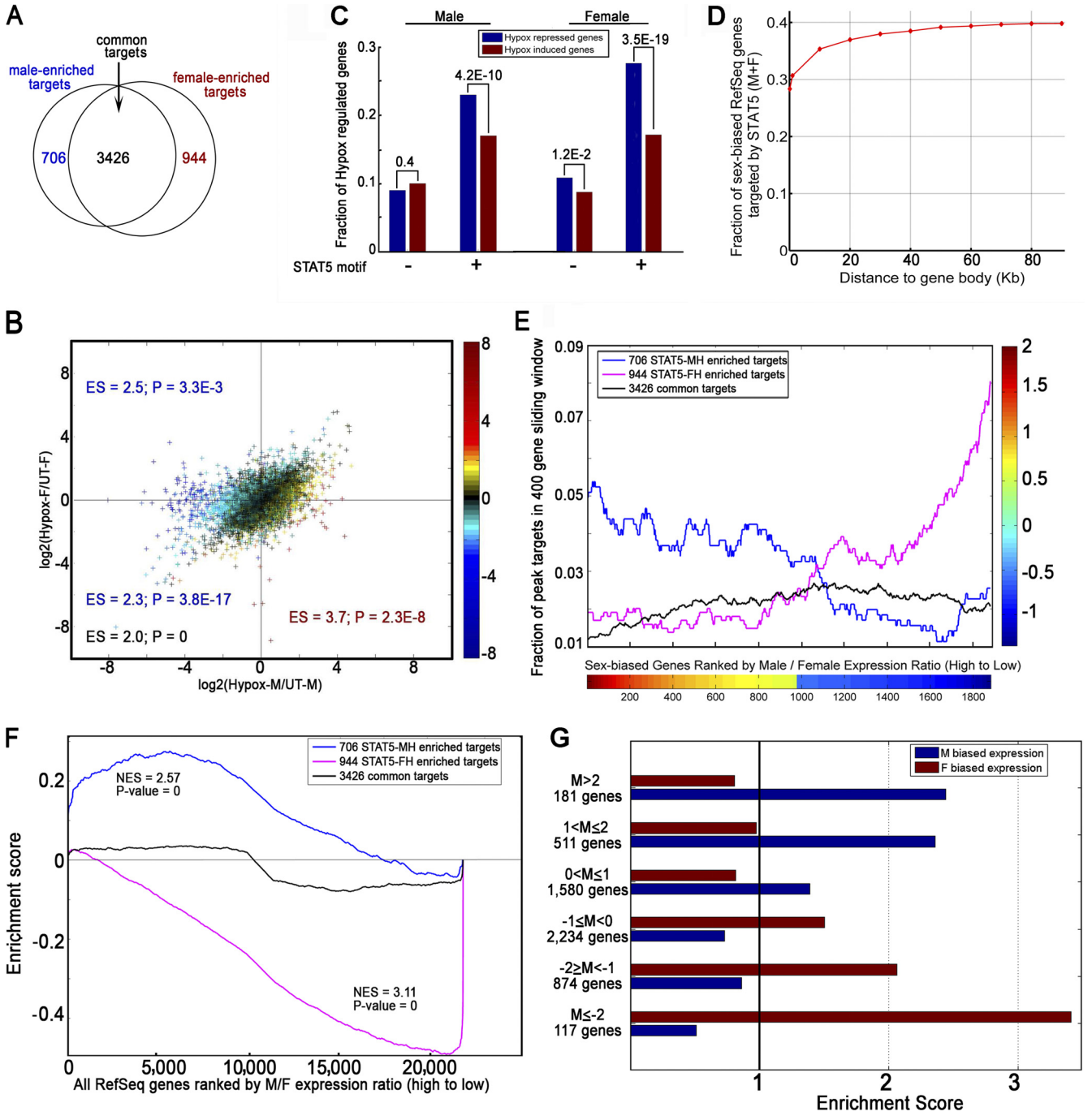

FIG 4 Relationship between sex-enriched STAT5 binding and pituitary GH-dependent and sex-biased gene expression. (A) The set of 15,094 merged STAT5 peaks (Fig. 3A) was mapped to STAT5 target genes, defined as RefSeq genes within 10 kb of a merged STAT5 peak. A total of 10,617 (70%) of the 15,094 STAT5 peaks mapped to a total of 5,076 genes, which were classified as male-enriched, female-enriched, or common STAT5 targets, as indicated in the Venn diagram. (B) Enrichment of each of the 3 sets of STAT5 targets shown in panel A for genes that respond to hypophysectomy (Hypox) in either male or female mouse liver. The graph shows the changes in gene expression following hypophysectomy in male versus female liver, and it is based on microarray data (61). Data are graphed as the $\log_2$ expression ratios for hypophysectomized versus untreated controls (UT; i.e., sham-operated mice) in males (*x* axis) and females (*y* axis) for genes that passed the microarray significance filter of $P < 0.001$. Each point represents one gene, and the color indicates its female/male expression ratio in untreated mouse liver, as indicated in the $\log_2$-scale color bar at the right. Shown are ESs and Fisher exact test *P* values calculated for each of the three STAT5 target gene sets in panel A in the sets of genes that fell into each quadrant, using all RefSeq genes represented on the microarray as background. Blue lettering indicates ES values for STAT5-MH-enriched targets, brown lettering indicates ES values for STAT5-FH-enriched targets, and black lettering indicates ES values for STAT5 male and female common targets. The finding of STAT5 target genes significantly enriched in all but the first quadrant, which represents genes induced by hypophysectomy in both male and female liver, is consistent with GH-activated STAT5 primarily being a positive regulator of gene expression. (C) Genes that respond to hypophysectomy at a *P* level of <0.001 are enriched in STAT5 targets that contain a STAT5 motif, in both male liver (left) and female (right) liver. Nearly identical results were obtained using other cutoffs to define hypophysectomy-responsive genes (data not shown). (D) Fraction of sex-biased RefSeq genes that are targeted by STAT5 as a function of distance from STAT5 peak to gene body used to identify the gene as a STAT5 target. (E) A total of 2,282 sex-biased

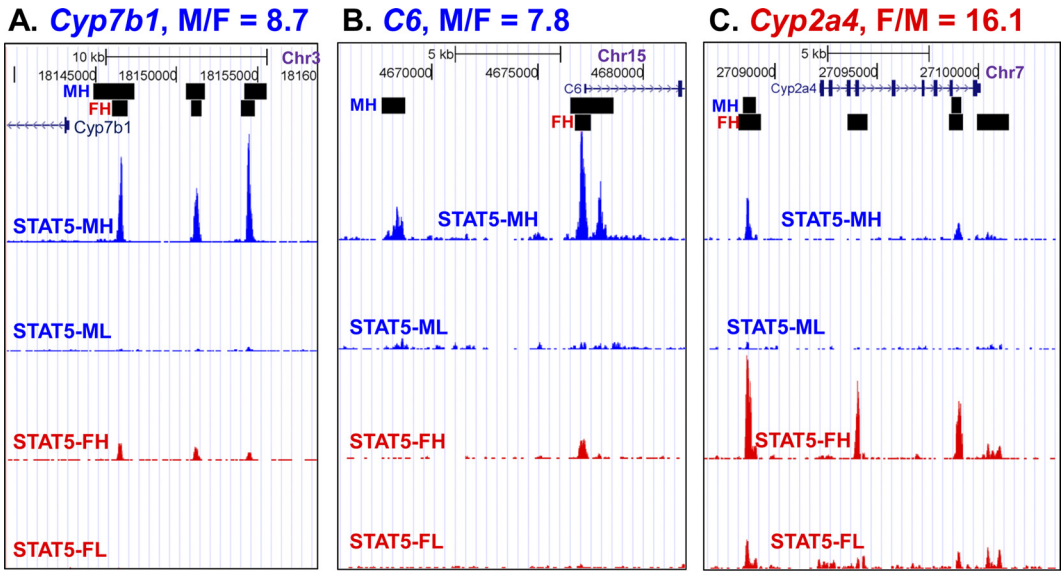

FIG 5 Sex-biased binding of STAT5 at sex-specific genes. Shown are UCSC Genome Browser screen shots with examples of male-enriched binding of STAT5 at male-specific genes (A and B) and female-enriched binding of STAT5 at a female-specific gene (C). Each panel shows the sex specificity of each gene (male/female or female/male expression ratio) as determined by microarray analysis (61), with horizontal black bars indicating the chromosomal intervals found to contain binding sites for STAT5 in STAT5 high-activity male (MH) and female (FH) livers. The bottom four tracks show the STAT5 ChIP-Seq reads for the four indicated mouse groups, as shown in Fig. 1D.

STAT5 targets showed female-biased expression (right side of graph), and no sex bias in expression was observed for STAT5 common targets (black curve). This conclusion was supported by gene set enrichment analysis, which showed that male-enriched STAT5 targets are significantly enriched in male-biased genes and correspondingly for female-enriched STAT5 targets (Fig. 4F). Finally, to investigate the relationship between the degree of sex specificity of STAT5 binding (i.e., magnitude of the M value) and the enrichment of sex-specific genes, we applied a range of cutoff values to obtain 6 subsets of sex-dependent STAT5 peaks (see Fig. S4 in the supplemental material); ES values for sex-specific targets were then calculated for each subset. The enrichment score for male-biased genes increased substantially with increasing male/female ratio of STAT5 binding activity, and the ES increased similarly for female-biased genes and increasing female/male ratio of STAT5 binding (Fig. 4G).

BCL6-M targets overlap with STAT5 targets and are enriched in female-biased genes. BCL6 is a male-biased transcriptional repressor (43) that can bind to STAT5 consensus sequences and inhibit STAT5-dependent gene expression (6, 7, 43). The repressive activity of BCL6 was observed in a reporter assay, where BCL6 strongly repressed GH- and STAT5-dependent *trans*-activation of a STAT5-responsive sequence upstream of *Cyp2c12* (18), a highly female-specific, GH-regulated gene (see Fig. S5A in the supplemental material). STAT5, in turn, can repress the expression of *BCL6*, with repression being more complete in female than in male liver due to the more persistent activation of STAT5 by the female plasma GH profile (43). Using ChIP-Seq, we identified 6,432 BCL6 peaks in male liver (BCL6-M) versus only 909 peaks in female liver (BCL6-F) (Table 1; see also Table S1G and H in the supplemental material), consistent with the higher expression of BCL6 in male liver. We did not observe a clear relationship between the STAT5 activity status of a given liver and the number of BCL6 peaks obtained by ChIP-Seq, reflecting the inconsistent relationship between STAT5 activity and BCL6 protein levels in individual livers (43). This conclusion was supported by a ChIP-qPCR assay of BCL6 binding activity at select BCL6 binding sites in STAT5 low-activity compared to STAT5 high-activity livers (see Fig. S1C in the supplemental material).

Comparison of BCL6-M peaks with the full set of merged STAT5-MH peaks revealed a significant overlap (52%) (Fig. 6A). Seven subsets of peaks were identified (classes I to VII) (Fig. 6A; see also Table S2B in the supplemental material). *De novo* motif discovery yielded distinct motifs in the BCL6 unique peak set (class VII) compared to the STAT5 unique peak sets (classes I to III) (Fig. 6B; see also Fig. S5B in the supplemental material), with binding requirements of the BCL6 unique peak set being more restricted in the central positions and more relaxed in the outer positions in relation to the STAT5 motif. The STAT5 and BCL6 common peaks (classes IV to VI) were described by motifs inter-

RefSeq genes were ranked based on male/female expression ratio, as shown in the color bar at the bottom ($\log_2$ ratios). For each of the three sets of STAT5 target genes shown in panel A, the fraction of targets present in each consecutive set of 400 sex-biased genes was calculated. The frequency of STAT5 target genes increased dramatically with increasing expression sex bias, most noticeably for the female-specific genes (right). (F) Gene set enrichment analysis showing a significant NES (normalized enrichment score) for STAT5-MH-enriched targets in male-biased genes and for STAT5-FH-enriched targets in female-biased genes. The *x* axis represents all 21,794 RefSeq genes present on the Agilent 44K_v1 microarray platform used to obtain the male/female expression ratios (61); the *y* axis presents the running enrichment score. (G) Enrichment of male-specific and female-specific genes in six sets of STAT5 targets, which were identified using six subsets of STAT5 peaks, as defined by the indicated ranges of normalized $\log_2$ male/female STAT5 sequence reads (M-values) and as shown in Fig. S4 of the supplemental material.

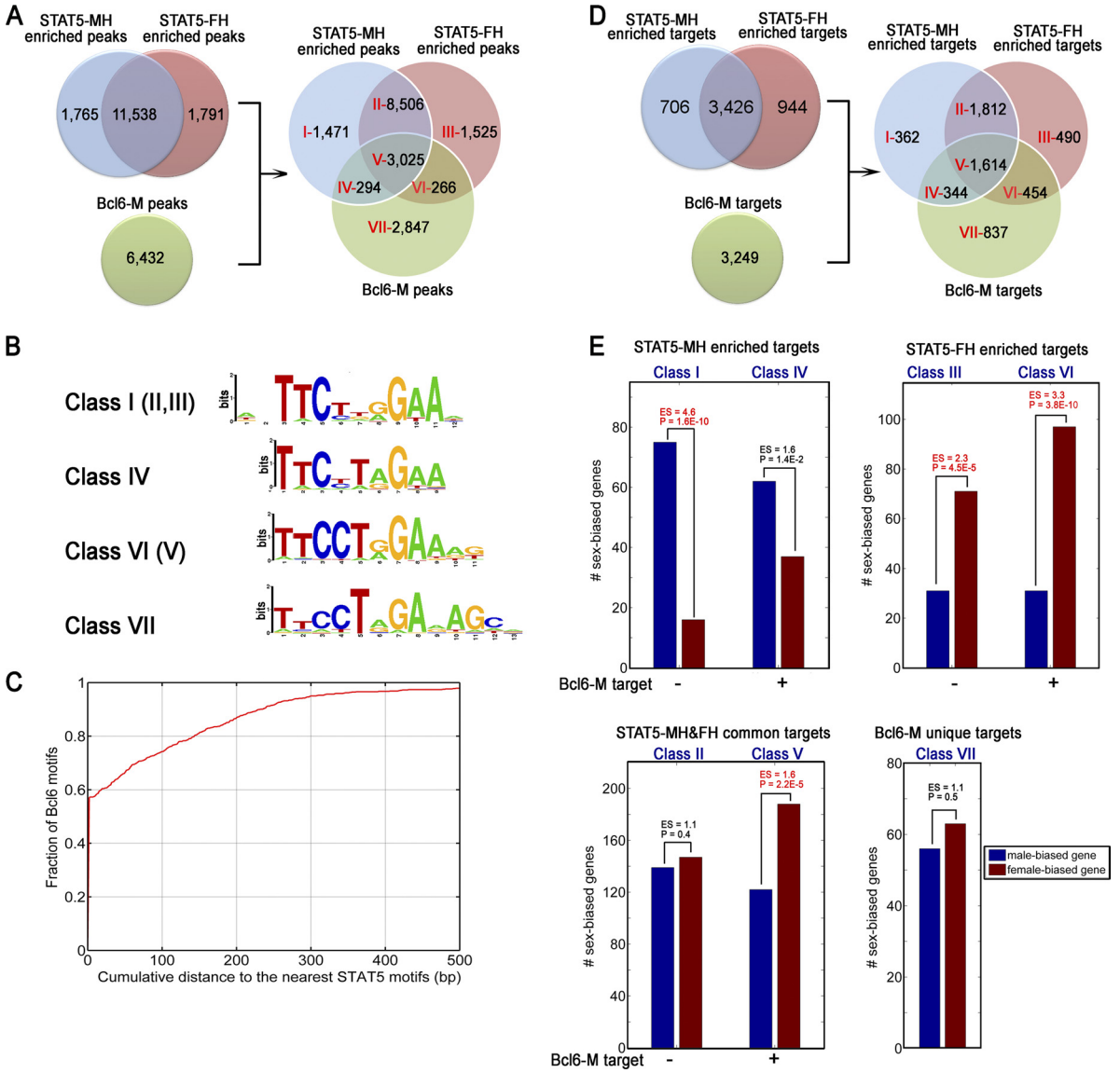

FIG 6 The seven classes of STAT5 and BCL6 binding sites: motifs, targets, and enrichment for sex-specific genes. (A) Venn diagrams depicting the number of peaks that overlapped between the indicated STAT5 and BCL6-M peak sets, as determined by comparing the genomic coordinates (see Table S1 in the supplemental material). (B) The DNA sequence logos (motifs) for the seven different classes of STAT5 and BCL6 binding sites defined by the Venn diagram in panel A (labeled I to VII), identified by *de novo* motif discovery. Motif discovery was carried out using peaks trimmed to a total width of 600 nt centered around the peak summit. The motif shown for class I sites is almost identical to the motifs for classes II and III, and the motif shown for class VI sites is almost identical to the motif for class V, as indicated (see also Fig. S5B in the supplemental material). (C) Cumulative distribution of the distance from the BCL6 motif to the nearest STAT5 motif for the set of STAT5 and BCL6 common peaks (i.e., classes IV, V, and VI in panel A) that contained both motifs. (D) Venn diagrams depicting the number of gene targets that overlapped between the indicated STAT5 and BCL6-M target gene sets. The target gene sets identified by this Venn diagram are designated I to VII and correspond to the seven peak sets shown in panel A. (E) Enrichment of male-specific genes versus female-specific genes in each of the indicated seven classes of STAT5 and BCL6 targets, as marked and based on the target gene sets shown in panel D. ESs and Fisher exact test *P* values are shown on the top of each bar set.

mediate to those of the STAT5 unique and BCL6 unique peak sets. Finally, STAT5 and BCL6 binding occurred in close proximity: in 57% of the STAT5 and BCL6-M common peaks that contained both motifs, the motifs overlapped within 2 bp (Fig. 6C).

The set of 6,432 BCL6-M peaks mapped to 3,249 RefSeq gene targets in male liver. These BCL6-M targets were significantly enriched in female-biased genes compared to male-biased genes (ES, 1.44; $P = 1.5E-7$). A majority (74%) of the BCL6 targets were also targets of STAT5, accounting for 48% of STAT5 targets (Fig. 6D; see also Table S2C in the supplemental material). Comparison of BCL6 targets with the three subsets of STAT5 targets identified above (male-enriched, female-enriched, and STAT5 common targets) identified seven classes of target genes (Fig. 6D, right). Figure 6E shows that STAT5 and BCL6 common targets (classes IV to VI) had a greater enrichment of female-biased versus male-biased genes than the corresponding STAT5 unique targets (i.e., class IV versus class I, class VI versus class III, and class V versus class II). BCL6 unique targets (class VII) showed no sex bias, perhaps due to the low intensity of BCL6 binding in this group. The overall enrichment of female-biased compared to male-biased genes in

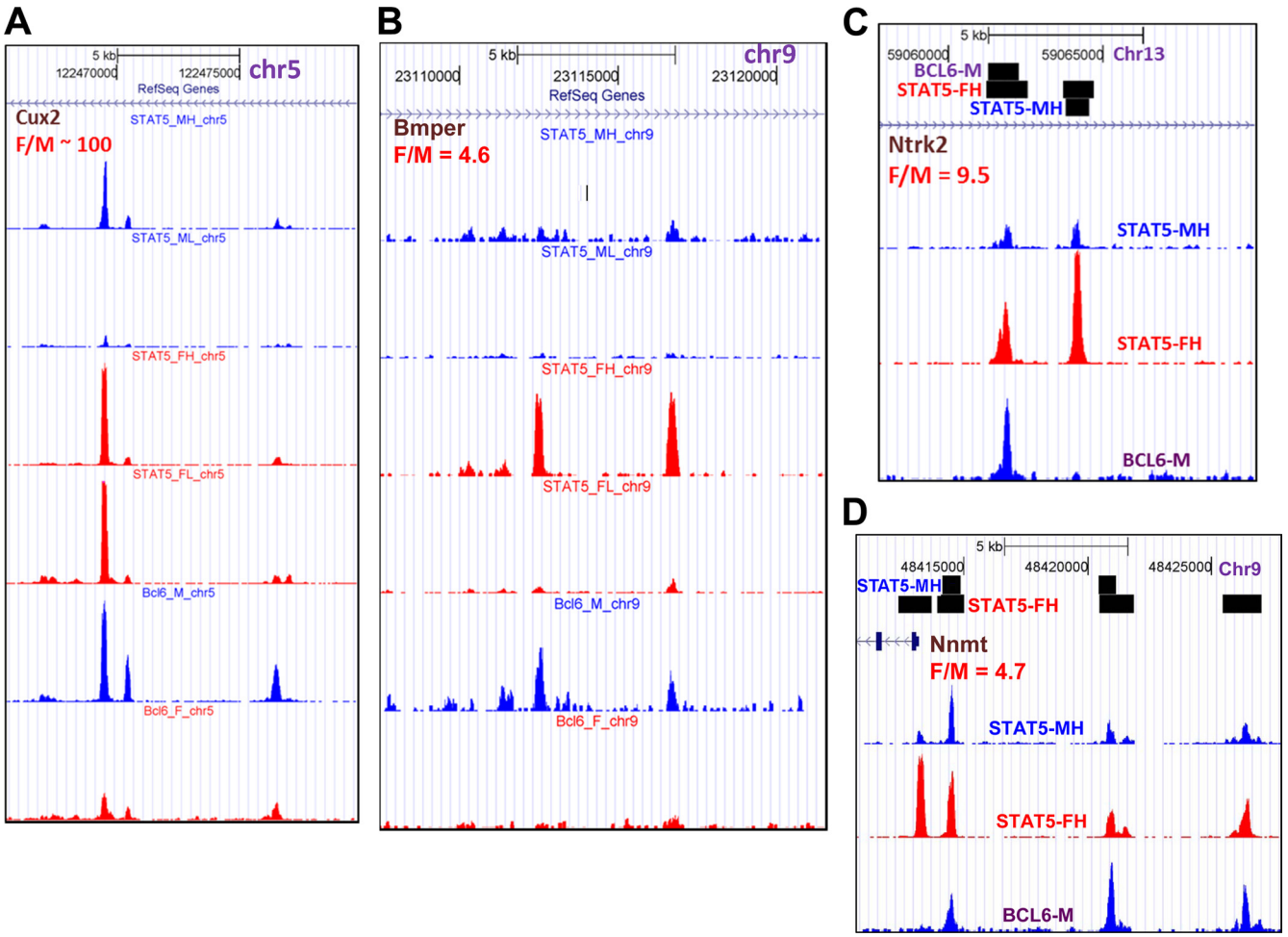

FIG 7 BCL6 binding in male liver at sites associated with female-enriched STAT5 binding to female-specific genes. Shown are UCSC Browser screen shots of STAT5 and BCL6 binding to the four female-specific genes, *Cux2*, *Bmper*, *Ntrk2*, and *Nnmt*. (A and B) The same four tracks of STAT5 binding shown in Fig. 5, plus two additional tracks that showed BCL6 binding in male and female liver, as marked above each track. (C and D) Screen shots for the three indicated tracks only, with horizontal bars marking the peak regions for the indicated tracks, as identified with MACS peak-calling software. Lower levels of STAT5 and BCL6 binding than those seen here were apparent in the STAT5-ML, STAT5-FL, and BCL6-F tracks (see data presented in Fig. S1E of the supplemental material). *Cux2* (A) belongs to STAT5/BCL6 class V, and the other three genes belong to class VI (Fig. 6D; see also Table S2C and D in the supplemental material). STAT5 binding persists in STAT5-FL liver compared to STAT5-FH liver in the case of *Cux2* (A) and other genes (see Fig. S1E), whereas STAT5 binding rarely persists in STAT5-ML liver compared to STAT5-MH liver. The female-to-male expression ratios shown were determined by microarray analysis (61), except for that for *Cux2*, which was determined by qPCR (35).

BCL6 and STAT5 common targets (classes IV to VI; ES, 1.52 and $P = 1E-7$) further supported a role for BCL6 in repressing STAT5-dependent female-biased genes in male liver. Examples of female-specific genes preferentially targeted by STAT5 in female liver but by BCL6 in male liver are shown in Fig. 7 (see also Fig. S1E in the supplemental material).

Motifs for other liver transcription factors associated with STAT5 and BCL6 binding sites. Next, we analyzed the 7 classes of STAT5 and BCL6 peaks (Fig. 6A, right) to identify transcription factor motifs enriched in each peak set. As expected, STAT5 motifs were highly enriched in all 6 classes of STAT5 peaks (classes I to VI), and BCL6 motifs were highly enriched in BCL6 peaks (classes IV to VII) (Fig. 8A). In addition, *de novo* motif discovery identified motifs representing the HNF6/CDP and HNF4/PPAR families in the STAT5 and BCL6 peaks sets, with some differences in the motifs discovered in the 7 peak classes apparent (see Fig. S5C and D in the suppplemental material; details are shown in Table S1 of the supplemental material). The HNF6/CDP motif showed greater enrichment in all STAT5 male peak sets (i.e., classes I, II, IV, and V), compared to peaks from other classes, consistent with our finding that HNF6/CDP motifs are strongly associated with male-enriched STAT5 binding (Fig. 3C). Furthermore, HNF4/PPAR motifs were most significantly enriched in peaks common to BCL6-M, STAT5-MH, and STAT5-FH (class V) (Fig. 8A). Consistently, when we mapped a published HNF4 ChIP-Seq peak list for male mouse liver (51) to our ChIP-Seq peaks, 73% of class V peaks overlapped with HNF4 binding sites (see Fig. S5E). Together, these findings indicate that HNF6/CDP factors are associated with STAT5 binding in male liver, while HNF4/PPAR factors are associated with STAT5 (and BCL6) binding in both male and female liver. Several other motifs were preferentially enriched in STAT5-MH-enriched and BCL6-M common (class IV) peaks (Fig. 8A).

GO enrichment analysis. STAT5 and BCL6 common target

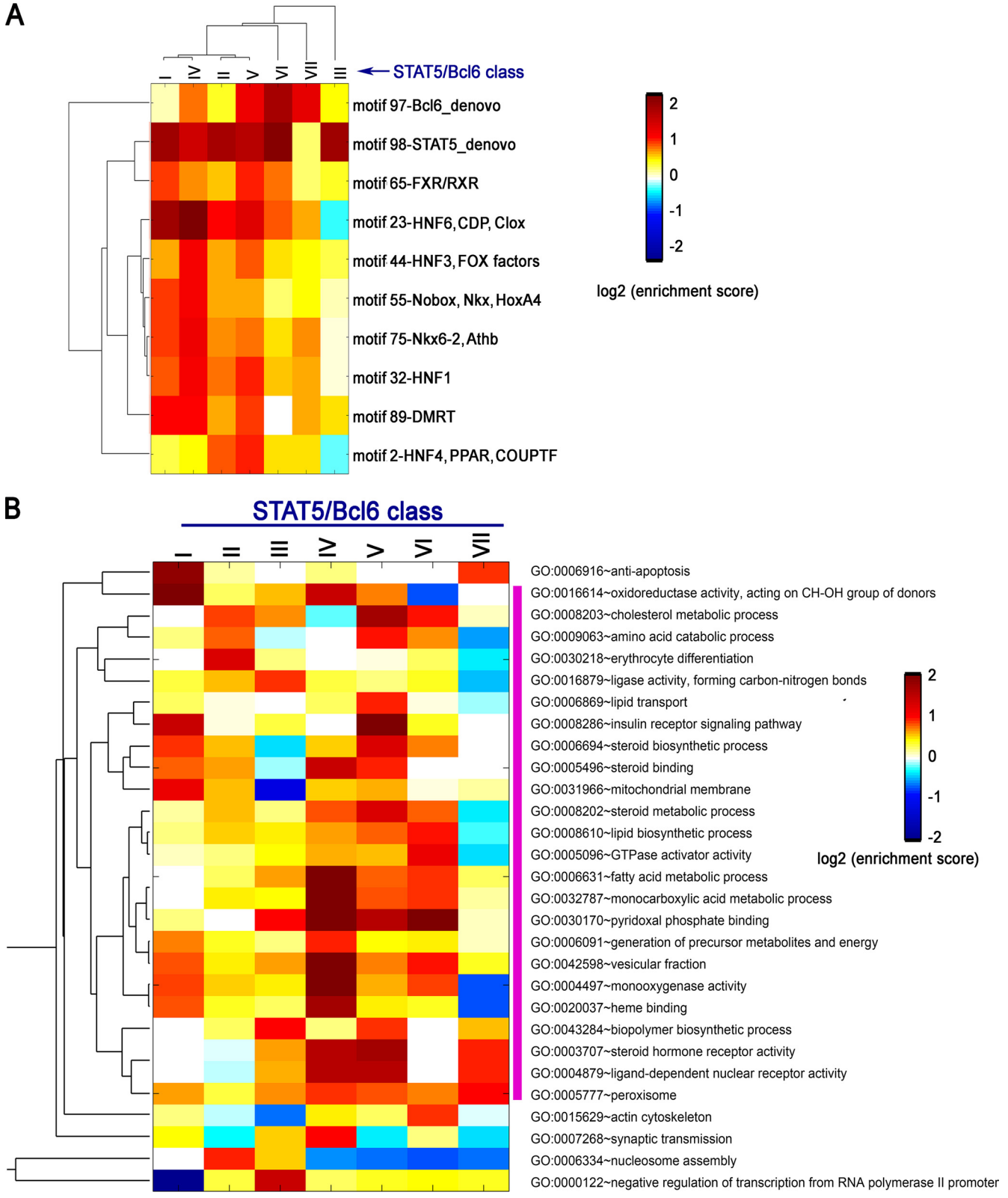
A
I
IV
II
V
VI
VII
III
STAT5/Bcl6 class
motif 97-Bcl6_denovo
motif 98-STAT5_denovo
motif 65-FXR/RXR
motif 23-HNF6,CDP,Clox
motif 44-HNF3,FOX factors
motif 55-Nobox, Nkx, HoxA4
motif 75-Nkx6-2,Athb
motif 32-HNF1
motif 89-DMRT
motif 2-HNF4,PPAR,COUPTF
2
1
0
-1
-2
log2 (enrichment score)
B
STAT5/Bcl6 class
I
II
III
IV
V
VI
VII
GO:0006916~anti-apoptosis
GO:0016614~oxidoreductase activity, acting on CH-OH group of donors
GO:0008203~cholesterol metabolic process
GO:0009063~amino acid catabolic process
GO:0030218~erythrocyte differentiation
GO:0016879~ligase activity, forming carbon-nitrogen bonds
GO:0006869~lipid transport
GO:0008286~insulin receptor signaling pathway
GO:0006694~steroid biosynthetic process
GO:0005496~steroid binding
GO:0031966~mitochondrial membrane
GO:0008202~steroid metabolic process
GO:0008610~lipid biosynthetic process
GO:0005096~GTPase activator activity
GO:0006631~fatty acid metabolic process
GO:0032787~monocarboxylic acid metabolic process
GO:0030170~pyridoxal phosphate binding
GO:0006091~generation of precursor metabolites and energy
GO:0042598~vesicular fraction
GO:0004497~monooxygenase activity
GO:0020037~heme binding
GO:0043284~biopolymer biosynthetic process
GO:0003707~steroid hormone receptor activity
GO:0004879~ligand-dependent nuclear receptor activity
GO:0005777~peroxisome
GO:0015629~actin cytoskeleton
GO:0007268~synaptic transmission
GO:0006334~nucleosome assembly
GO:0000122~negative regulation of transcription from RNA polymerase II promoter
2
1
0
-1
-2
log2 (enrichment score)

genes (classes IV to VI) were highly enriched in GO terms related to lipid metabolism and cytochrome P450 metabolism/monooxygenase activity, among other terms (Fig. 8B, inner black rectangle). STAT5 unique targets (classes I to III) were only moderately enriched, and BCL6 unique targets (class VII) were generally depleted of these terms (Fig. 8B; see also Table S3 in the supplemental material). This suggests that BCL6 impacts the regulation of hepatic lipid metabolism through its effects on STAT5 and BCL6 common target genes. Class III genes, which represent targets of female-enriched STAT5 binding sites, were significantly enriched in genes associated with negative regulation of transcription from RNA polymerase II promoters (see Table S3), among others. Genes with a sex-independent STAT5 binding site and without a BCL6 binding site (class II) showed enrichment for nucleosome assembly, suggesting a close association between STAT5 binding and chromatin structure remodeling. Interestingly, the STAT5 sequence read density around the histone genes that comprise this GO term were comparable between the STAT5-low and STAT5-high livers in both males and females (see Fig. S1E in the supplemental material). BCL6 unique peak targets showed highest enrichment for peroxisomal genes, consistent with the cooperative role that BCL6 plays with the peroxisome proliferator-activated receptor (PPAR) in target gene regulation (31, 49). Strong enrichment for antiapoptosis genes was also seen, consistent with BCL6 inhibition of apoptotic cell death (32).

DISCUSSION

The tight regulation of hundreds of sex-biased genes in response to the pattern of GH input signals (pulsatile in males, near continuous in females) is an intriguing biological phenomenon whose underlying molecular mechanism has been elusive. Presently, we identified intermittent (male) versus persistent (female) signaling by STAT5, a transcriptional activator previously implicated in the sex-dependent actions of GH, as a critical feature of GH-regulated liver sex differences. Furthermore, we characterized on a genome-wide scale the dynamic, sex-differential liver DNA binding profiles of STAT5 and those of BCL6, a male-predominant, GH-regulated transcription repressor whose binding sites overlap those of STAT5. In livers of mice killed at a peak of liver STAT5 activity, sex-differential STAT5 binding to chromatin was observed and was closely associated with sex-biased expression of STAT5 target genes. Moreover, sex-differential STAT5 binding was enriched at sex-specific DNase hypersensitivity sites, which mark open chromatin regions, and was positively correlated with sex-biased activating chromatin marks and negatively correlated with sex-biased repressive chromatin marks surrounding the STAT5 binding sites. We further found that BCL6 preferentially bound to STAT5 targets that showed female-biased expression, which enabled BCL6 to antagonize the stimulatory effects of STAT5 on these female-biased genes in male liver (Fig. 9). Finally, genes involved in lipid metabolism and drug metabolism were

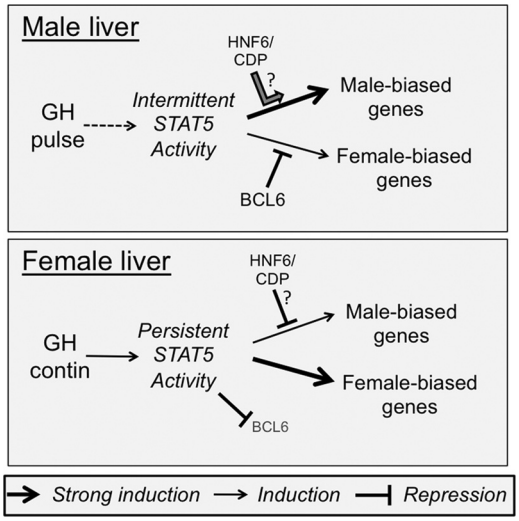

FIG 9 Model for regulation of sex-specific liver gene expression by STAT5, BCL6, and factor(s) with an HNF6/CDP motif. Male (pulsatile) plasma GH and female (near-continuous) plasma GH activate distinct temporal patterns of liver STAT5 activity (intermittent STAT5 activity in males versus persistent STAT5 activity in females) (Fig. 1A and B). These sex-differential patterns of liver STAT5 activity are, respectively, associated with male-enriched STAT5 binding at male-biased genes and female-enriched STAT5 binding at female-biased genes (Fig. 4). The transcriptional repressor BCL6 is more highly expressed in male liver, where it preferentially binds to STAT5 sites associated with female-biased genes (Fig. 6 and 7); this competition by BCL6 for STAT5 binding is proposed to augment liver sex differences by repressing the expression of female-biased genes in male liver. In female liver, where the female plasma GH profile suppresses *BCL6* (43), the repression of female-biased genes seen in male liver is relieved. Binding site motifs for HNF6/CDP factors are preferentially associated with male-enriched STAT5 binding sites (Fig. 3C), suggesting that an HNF6/CDP factor(s) contributes to the regulation of male-biased genes. Two possible mechanisms for this regulation are illustrated: (i) in male liver, an HNF6/CDP factor, perhaps HNF6 (ONECUT1), cooperates with STAT5 in positively regulating male-biased genes (top); (ii) in female liver, the HNF6/CDP family member CUX2 (CUTL2), which has been characterized as a repressor (21) that is expressed in female but not male liver (35), binds nearby male-enriched STAT5 binding sites and inhibits the expression of male-biased genes (bottom).

shown to be highly enriched in BCL6 and STAT5 common targets, but not in BCL6 unique targets, suggesting BCL6 plays a specific role in modulating GH/STAT5 regulation of these liver metabolic processes. This is the first study to elucidate genome-wide the dynamic, sex-differential binding of key transcription factors involved in sex-biased gene expression in a mammalian tissue *in vivo*, increasing our understanding of the mechanisms that govern the transcriptional and epigenetic regulation of hormone-dependent sex differences.

Dynamic, GH-regulated STAT5 binding to target genes. Our finding of ~9,800 liver STAT5 binding sites in male mice killed at a peak of STAT5 activity (STAT5-high liver) versus only ~800

FIG 8 Transcription factor motif (A) and gene ontology (B) enrichment analysis for 7 sets of STAT5 and BCL6 peak targets. (A) Heat map showing ES values of all motifs enriched ($P < 1E-10$; ES, >1.7) in at least 1 set of the 7 peak sets shown in Fig. 6A, using as background the motifs present in all mouse liver DHS sites (39) that showed no overlap with STAT5-MH or STAT5-FH peaks or BCL6-M peaks. The motif families used for enrichment analysis were the set of 97 motif families described previously (41), supplemented with additional motifs as described in Materials and Methods. (B) Heat map showing ES values for GO terms meeting the combined threshold of ES of >2.5 and P of <0.01, and the number of genes in each gene list containing >8 in at least 1 of the 7 gene sets defined in Fig. 6D, using all RefSeq genes as background. Genes in each of the 7 gene sets that had enriched GO terms are listed in Table S3 of the supplemental material. Dark red represents highly enriched GO terms, white indicates no enrichment, and blue indicates depletion of the GO term from the indicated gene set, as specified by the ES scale color bar at the right. The vertical pink bar at the right delineate GO terms associated with BCL6 and STAT5 common targets (classes IV to VI).

sites in male mice killed between STAT5 activity peaks (STAT5-low liver) indicates that STAT5 binds dynamically to thousands of sites genome-wide, most likely in direct response to each male plasma GH pulse. Many more liver STAT5 binding sites were found in STAT5-low females (~4,400 sites) than STAT5-low males (~800 sites), reflecting the higher basal circulating GH level and the persistence of liver STAT5 activity in females. A subset of the STAT5 binding sites identified in STAT5-high mouse liver was associated with genes induced rapidly by GH (see Table S2A in the supplemental material); however, the majority of STAT5 target genes identified here do not show rapid GH-stimulated transcriptional responses *in vivo* (61), suggesting their expression is codependent on factors downstream of GH-activated STAT5 binding or on factors derived from other GH-activated signaling pathways (34). The early GH-responsive STAT5 targets include *Igf1*, *Socs2*, and *Cish*, which rapidly recruit STAT5 following GH stimulation in both mouse and rat liver (7, 17, 36). STAT5 binding to *Socs2* and *Cish* is concentrated in promoter regions (see Fig. S1E); in contrast, STAT5 binding sites near *Igf1* are dispersed over an ~140-kb region, extending from the far upstream region to the promoter and across the entire gene body (Fig. 1D). Given our finding that STAT5 binding to these targets is dynamic and likely to result directly from the repeated cycles of STAT5 activation and deactivation that follow each pulse of circulating GH, as seen in rat liver (10, 59), transcription of these early STAT5 response genes may follow the same pulsatile rhythm as plasma GH stimulation.

Role of STAT5 in sex-specific liver gene expression. STAT5, in particular STAT5b, is essential for ~90% of sex-biased liver gene expression, as shown in STAT5-deficient mouse models (11, 26). However, it was unclear whether STAT5 directly regulates the hundreds of sex-biased genes that are STAT5b dependent, given that direct STAT5 target genes, such as *Igf1*, do not show significant sex-biased expression. Indeed, there was very little evidence of direct binding of STAT5 to regulatory regions associated with sex-specific genes (18, 20, 36), raising the possibility that the effects of STAT5 on sex-specific gene expression might largely be indirect (63). However, the present study demonstrates that direct STAT5 binding to sex-biased genes is widespread, with 35 to 40% of sex-biased genes serving as STAT5 targets, including both male-specific and female-specific genes (see Table S2D in the supplemental material). Moreover, STAT5 showed sex-differential binding at many (41%) of its sex-specific targets. In contrast, no sex differences in STAT5 binding were seen at *Igf1* (Fig. 1D) or many other sex-independent genes. Furthermore, male-enriched STAT5 binding sites were preferentially associated with male-biased genes and, correspondingly, for female-enriched STAT5 binding sites and female-biased genes (see examples in Fig. 5), indicating that STAT5 plays a positive regulatory role. The widespread downregulation of male-specific genes in STAT5b knockout male mouse liver (11) is consistent with positive regulation by STAT5. Although many female-specific genes are not downregulated in STAT5b knockout female mouse liver (11), this could reflect a compensatory role of STAT5a, which although expressed at much lower levels than STAT5b, is able to play a unique role in supporting female-specific liver gene expression (12). We also observed male-enriched STAT5 binding for some female-biased genes, as well as female-enriched STAT5 binding at some male-biased genes (see Table S2D and E in the supplemental material). This suggests that STAT5 can also impart negative regulation to sex-biased genes, consistent with reports of STAT5 transcription-inhibitory activity (14, 45, 71) and with the derepression of many female-specific genes seen in STAT5b-deficient male liver (11). Sex-biased genes that are STAT5 dependent (11, 26) but were not presently identified as targets of STAT5 binding may be regulated by distal STAT5 binding sites (i.e., >10 kb from gene body) or may be regulated by STAT5 by indirect mechanisms.

Mechanistic basis for sex differences in STAT5 binding. Many (24%) of the STAT5 binding sites that we identified in STAT5 high-activity livers showed sex-differential STAT5 binding, with weaker binding generally seen at the sex-dependent STAT5 binding sites compared to the sex-independent sites. Peaks of STAT5 activity were of similar intensities in male and female mouse liver (Fig. 1A), indicating that the sex differences in STAT5 binding at weaker STAT5 binding sites cannot be explained by differences in intranuclear STAT5 concentrations between sexes, in contrast to the situation in rat liver chromatin (36). Furthermore, no differences between sexes were apparent in the *de novo*-discovered STAT5 motifs associated with sex-dependent STAT5 binding sites or in their enrichment of the STAT5 motif. Motif differences were apparent, however, for the subset of sex-dependent STAT5 binding sites that also bind BCL6, as discussed further below. Moreover, we found that the male-enriched STAT5 binding sites are preferentially associated with HNF6/CDP motifs. One of the factors represented by the HNF6/CDP motif, CUX2, is a repressor that shows unusually high female-biased expression (~100-fold) in both mouse and rat liver (35). CUX2 could contribute to male-enriched STAT5 binding at male-biased genes by inhibiting STAT5 binding in female liver (Fig. 9, bottom), either directly or via epigenetic modifications that it induces. We did observe differences between sexes in chromatin structure surrounding the sex-dependent STAT5 binding sites, with male-enriched STAT5 sites being more open, relatively enriched in H3-K4me1 and H3-K4me3 (activating) marks, and relatively depleted of H3-K27me3 and to a lesser extent H3-K9me3 (repressive) marks in male liver than female-enriched STAT5 sites, and vice versa for female-enriched STAT5 sites. Differences between sexes in mouse liver chromatin structure are regulated globally by the sex-dependent patterns of circulating GH, as indicated by DNase hypersensitivity analysis (39). Moreover, acute GH stimulation can induce local changes in histone acetylation and methylation (7).

Repression of female-biased STAT5 targets by BCL6. BCL6 binding sites were 7-fold more numerous in male than female mouse liver, consistent with the male-biased expression of liver BCL6 (43). A substantial fraction (52%) of the BCL6 binding sites identified overlapped with binding sites for STAT5 in male liver, indicating a role for BCL6 in repressing STAT5 targets in male liver via its potent repressor activity. The STAT5 targets bound by BCL6 were enriched in female-biased genes, suggesting that BCL6 preferentially represses female-biased genes in male liver (Fig. 9, top). STAT5 and BCL6 were bound to distinct but overlapping sequence motifs, supporting the proposal that STAT factors and BCL6 directly compete for DNA binding (15, 16, 23). Distinct motifs also characterized BCL6 binding sites that overlapped male-enriched compared to female-enriched STAT5 binding sites (class IV versus class VI motifs) (Fig. 6B). BCL6 repression could thus involve direct competition for STAT5 binding, as well as repressive epigenetic modifications induced by BCL6-associated factors. Indeed, we observed an increase in H3-K27me3 (repressive) marks surrounding BCL6 binding sites in male but not fe-

male liver (see Fig. S5F and G in the supplemental material), although there was no corresponding sex difference in chromatin accessibility (see Fig. S5H and I). In B cells, BCL6 recruits class II histone deacetylases (37), while histone acetyltransferases act as transcriptional coactivators that reverse this action by inactivation of BCL6 (47).

Association between HNF4A binding and STAT5 binding sites. Sex differences in nuclear receptor-regulated liver metabolic pathways have been described (48), but their relationship to STAT5 action is obscure. A large fraction of sex-biased genes respond in parallel to the loss of STAT5 and HNF4A in male liver, indicating a codependence and suggesting that these two factors coregulate sexually dimorphic liver gene expression (27, 28, 46). Here, nuclear receptor motifs related most closely to those of HNF4A and the nuclear receptor PPAR were identified *de novo* as significantly enriched near STAT5 and BCL6 binding sites. Many of these motifs are functional in binding HNF4A, as revealed by our examination of the overlap between HNF4A binding sites in male mouse liver (51) and the 7 classes of STAT5/BCL6-M sites defined here: 41% of mouse liver HNF4A binding sites overlapped with one of the 7 classes of STAT5/BCL6-M peaks, and they accounted for 47% of STAT5 and BCL6-M peaks. Of note, 73% of class V peaks (Fig. 6A), which are bound by BCL6 in male liver and by STAT5 in both male and female liver, were also bound by HNF4A in male liver (see Fig. S5E in the supplemental material). Importantly, each of the seven STAT5/BCL6 binding site classes was associated with a distinct HNF4/PPAR family motif (see Fig. S5C), suggesting that they have distinct binding potential for HNF4A, PPAR, or other family members. Further study is required to determine the significance of these motif differences, as well as the significance of the STAT5-associated HNF6/CDP sites discussed above, in particular, their impact on the observed sex dependence and differential binding of STAT5 and BCL6 that occurs at these sites.

Conclusions. This study elucidated the genome-wide sex-differential binding of two key factors involved in sex-biased gene expression in a mammalian tissue *in vivo*; it provides a comprehensive view of the mechanisms whereby GH-regulated transcription factors establish and maintain sex-differential transcription in the liver, and it enhances our understanding of sex differences affecting liver physiology and disease.

ACKNOWLEDGMENTS

This work was supported by Public Health Service grant DK-33765 from the National Institutes of Health (to D.J.W.).

We thank Aarathi Sugathan of our laboratory and Ernest Fraenkel (Department of Biological Engineering, MIT) and Stuart Levine (Biomicro Center, MIT) for useful discussions.

There are no competing interests to be declared.

D.J.W. conceived and designed the experiments; E.V.L. performed the laboratory-based studies; Y.Z. analyzed the ChIP-Seq data and prepared figures and tables for publication; Y.Z. and D.J.W. wrote the manuscript.

REFERENCES

1. **Ayonrinde OT, et al.** 2011. Gender-specific differences in adipose distribution and adipocytokines influence adolescent nonalcoholic fatty liver disease. Hepatology **53**:800–809.
2. **Baik M, Yu JH, Hennighausen L.** 2011. Growth hormone-STAT5 regulation of growth, hepatocellular carcinoma, and liver metabolism. Ann. N. Y. Acad. Sci. **1229**:29–37.
3. **Bannister AJ, Kouzarides T.** 2011. Regulation of chromatin by histone modifications. Cell Res. **21**:381–395.
4. **Bhadhprasit W, Sakuma T, Kawasaki Y, Nemoto N.** 2011. Hepatocyte nuclear factor 4α regulates expression of the mouse female-specific Cyp3a41 gene in the liver. Drug Metab. Dispos **39**:490–497.
5. **Chang CC, Ye BH, Chaganti RS, Dalla-Favera R.** 1996. BCL-6, a POZ/zinc-finger protein, is a sequence-specific transcriptional repressor. Proc. Natl. Acad. Sci. U. S. A. **93**:6947–6952.
6. **Chen Y, et al.** 2009. Computational and functional analysis of growth hormone (GH)-regulated genes identifies the transcriptional repressor B-cell lymphoma 6 (Bc16) as a participant in GH-regulated transcription. Endocrinology **150**:3645–3654.
7. **Chia DJ, Rotwein P.** 2010. Defining the epigenetic actions of growth hormone: acute chromatin changes accompany GH-activated gene transcription. Mol. Endocrinol. **24**:2038–2049.
8. **Chia DJ, Varco-Merth B, Rotwein P.** 2010. Dispersed chromosomal Stat5b-binding elements mediate growth hormone-activated insulin-like growth factor-I gene transcription. J. Biol. Chem. **285**:17636–17647.
9. **Choi HK, Waxman DJ.** 1999. Growth hormone, but not prolactin, maintains, low-level activation of STAT5a and STAT5b in female rat liver. Endocrinology **140**:5126–5135.
10. **Choi HK, Waxman DJ.** 2000. Plasma growth hormone pulse activation of hepatic JAK-STAT5 signaling: developmental regulation and role in male-specific liver gene expression. Endocrinology **141**:3245–3255.
11. **Clodfelter KH, et al.** 2006. Sex-dependent liver gene expression is extensive and largely dependent upon signal transducer and activator of transcription 5b (STAT5b): STAT5b-dependent activation of male genes and repression of female genes revealed by microarray analysis. Mol. Endocrinol. **20**:1333–1351.
12. **Clodfelter KH, et al.** 2007. Role of STAT5a in regulation of sex-specific gene expression in female but not male mouse liver revealed by microarray analysis. Physiol. Genomics **31**:63–74.
13. **Davey HW, et al.** 2001. STAT5b is required for GH-induced liver IGF-I gene expression. Endocrinology **142**:3836–3841.
14. **Delesque-Touchard N, Park SH, Waxman DJ.** 2000. Synergistic action of hepatocyte nuclear factors 3 and 6 on CYP2C12 gene expression and suppression by growth hormone-activated STAT5b. Proposed model for female specific expression of CYP2C12 in adult rat liver. J. Biol. Chem. **275**:34173–34182.
15. **Dent AL, Shaffer AL, Yu X, Allman D, Staudt LM.** 1997. Control of inflammation, cytokine expression, and germinal center formation by BCL-6. Science **276**:589–592.
16. **Diehl SA, et al.** 2008. STAT3-mediated up-regulation of BLIMP1 is coordinated with BCL6 down-regulation to control human plasma cell differentiation. J. Immunol. **180**:4805–4815.
17. **Eleswarapu S, Gu Z, Jiang H.** 2008. Growth hormone regulation of insulin-like growth factor-I gene expression may be mediated by multiple distal signal transducer and activator of transcription 5 binding sites. Endocrinology **149**:2230–2240.
18. **Endo M, Takahashi Y, Sasaki Y, Saito T, Kamataki T.** 2005. Novel gender-related regulation of CYP2C12 gene expression in rats. Mol. Endocrinol. **19**:1181–1190.
19. **Franconi F, Brunelleschi S, Steardo L, Cuomo V.** 2007. Gender differences in drug responses. Pharmacol. Res. **55**:81–95.
20. **Gardmo C, Mode A.** 2006. In vivo transfection of rat liver discloses binding sites conveying GH-dependent and female-specific gene expression. J. Mol. Endocrinol. **37**:433–441.
21. **Gingras H, Cases O, Krasilnikova M, Berube G, Nepveu A.** 2005. Biochemical characterization of the mammalian Cux2 protein. Gene **344**:273–285.
22. **Gorski K, Carneiro M, Schibler U.** 1986. Tissue-specific in vitro transcription from the mouse albumin promoter. Cell **47**:767–776.
23. **Harris MB, Mostecki J, Rothman PB.** 2005. Repression of an interleukin-4-responsive promoter requires cooperative BCL-6 function. J. Biol. Chem. **280**:13114–13121.
24. **Hartatik T, et al.** 2001. Binding of BAZF and Bc16 to STAT6-binding DNA sequences. Biochem. Biophys. Res. Commun. **284**:26–32.
25. **Hennighausen L, Robinson GW.** 2008. Interpretation of cytokine signaling through the transcription factors STAT5A and STAT5B. Genes Dev. **22**:711–721.
26. **Holloway MG, et al.** 2007. Loss of sexually dimorphic liver gene expression upon hepatocyte-specific deletion of Stat5a-Stat5b locus. Endocrinology **148**:1977–1986.
27. **Holloway MG, Laz EV, Waxman DJ.** 2006. Codependence of growth hormone-responsive, sexually dimorphic hepatic gene expression on sig-

nal transducer and activator of transcription 5b and hepatic nuclear factor 4α. Mol. Endocrinol. **20**:647–660.
28. **Holloway MG, Miles GD, Dombkowski AA, Waxman DJ.** 2008. Liver-specific hepatocyte nuclear factor-4α deficiency: greater impact on gene expression in male than in female mouse liver. Mol. Endocrinol. **22**:1274–1286.
29. **Jansson JO, Eden S, Isaksson O.** 1985. Sexual dimorphism in the control of growth hormone secretion. Endocr. Rev. **6**:128–150.
30. **Ji H, et al.** 2008. An integrated software system for analyzing ChIP-chip and ChIP-seq data. Nat. Biotechnol. **26**:1293–1300.
31. **Kharroubi I, et al.** 2006. BCL-6: a possible missing link for anti-inflammatory PPAR-delta signalling in pancreatic beta cells. Diabetologia **49**:2350–2358.
32. **Kumagai T, et al.** 1999. The proto-oncogene Bc16 inhibits apoptotic cell death in differentiation-induced mouse myogenic cells. Oncogene **18**: 467–475.
33. **Lahuna O, et al.** 1997. Expression of hepatocyte nuclear factor 6 in rat liver is sex-dependent and regulated by growth hormone. Proc. Natl. Acad. Sci. U. S. A. **94**:12309–12313.
34. **Lanning NJ, Carter-Su C.** 2006. Recent advances in growth hormone signaling. Rev. Endocr. Metab. Disord. **7**:225–235.
35. **Laz EV, Holloway MG, Chen CS, Waxman DJ.** 2007. Characterization of three growth hormone-responsive transcription factors preferentially expressed in adult female liver. Endocrinology **148**:3327–3337.
36. **Laz EV, Sugathan A, Waxman DJ.** 2009. Dynamic in vivo binding of STAT5 to growth hormone-regulated genes in intact rat liver. Sex-specific binding at low- but not high-affinity STAT5 sites. Mol. Endocrinol. **23**: 1242–1254.
37. **Lemercier C, et al.** 2002. Class II histone deacetylases are directly recruited by BCL6 transcriptional repressor. J. Biol. Chem. **277**:22045–22052.
38. **Lichanska AM, Waters MJ.** 2008. How growth hormone controls growth, obesity and sexual dimorphism. Trends Genet. **24**:41–47.
39. **Ling G, Sugathan A, Mazor T, Fraenkel E, Waxman DJ.** 2010. Unbiased, genome-wide in vivo mapping of transcriptional regulatory elements reveals sex differences in chromatin structure associated with sex-specific liver gene expression. Mol. Cell. Biol. **30**:5531–5544.
40. **Logarajah S, et al.** 2003. BCL-6 is expressed in breast cancer and prevents mammary epithelial differentiation. Oncogene **22**:5572–5578.
41. **Macisaac KD, et al.** 2006. A hypothesis-based approach for identifying the binding specificity of regulatory proteins from chromatin immunoprecipitation data. Bioinformatics **22**:423–429.
42. **Margueron R, Reinberg D.** 2011. The Polycomb complex PRC2 and its mark in life. Nature **469**:343–349.
43. **Meyer RD, Laz EV, Su T, Waxman DJ.** 2009. Male-specific hepatic Bcl6: growth hormone-induced block of transcription elongation in females and binding to target genes inversely coordinated with STAT5. Mol. Endocrinol. **23**:1914–1926.
44. **Mode A, Gustafsson JA.** 2006. Sex and the liver: a journey through five decades. Drug Metab. Rev. **38**:197–207.
45. **Ono M, et al.** 2007. Signal transducer and activator of transcription (Stat) 5b-mediated inhibition of insulin-like growth factor binding protein-1 gene transcription: a mechanism for repression of gene expression by growth hormone. Mol. Endocrinol. **21**:1443–1457.
46. **Park SH, Wiwi CA, Waxman DJ.** 2006. Signalling cross-talk between hepatocyte nuclear factor 4α and growth-hormone-activated STAT5b. Biochem. J. **397**:159–168.
47. **Pasqualucci L, et al.** 2011. Inactivating mutations of acetyltransferase genes in B-cell lymphoma. Nature **471**:189–195.
48. **Rando G, Wahli W.** 2011. Sex differences in nuclear receptor-regulated liver metabolic pathways. Biochim. Biophys. Acta **1812**:964–973.
49. **Ravaux L, et al.** 2007. Inhibition of interleukin-1β-induced group IIA secretory phospholipase A2 expression by peroxisome proliferator-activated receptors (PPARs) in rat vascular smooth muscle cells: cooperation between PPARβ and the proto-oncogene BCL-6. Mol. Cell. Biol. **27**:8374–8387.
50. **Scandlyn MJ, Stuart EC, Rosengren RJ.** 2008. Sex-specific differences in CYP450 isoforms in humans. Expert Opin. Drug Metab. Toxicol. **4**:413–424.
51. **Schmidt D, et al.** 2010. Five-vertebrate ChIP-seq reveals the evolutionary dynamics of transcription factor binding. Science **328**:1036–1040.
52. **Schwartz JB.** 2007. The current state of knowledge on age, sex, and their interactions on clinical pharmacology. Clin. Pharmacol. Ther. **82**:87–96.
53. **Seyfert VL, Allman D, He Y, Staudt LM.** 1996. Transcriptional repression by the proto-oncogene BCL-6. Oncogene **12**:2331–2342.
54. **Shapiro BH, Agrawal AK, Pampori NA.** 1995. Gender differences in drug metabolism regulated by growth hormone. Int. J. Biochem. Cell Biol. **27**: 9–20.
55. **Su WL, et al.** 2008. Exon and junction microarrays detect widespread mouse strain- and sex-bias expression differences. BMC Genomics **9**:273.
56. **Subramanian A, et al.** 2005. Gene set enrichment analysis: a knowledge-based approach for interpreting genome-wide expression profiles. Proc. Natl. Acad. Sci. U. S. A. **102**:15545–15550.
57. **Sugathan A, Laz EV, Rampersaud A, Waxman DJ.** Role of histone-3 lysine 27 trimethylation (K27-me3) in repression of female-specific, growth hormone-regulated genes in male mouse liver. Endocr. Rev. **32**: P2–P330.
58. **Takemoto N, et al.** 2005. Sex-based molecular profiling of hepatitis C virus-related hepatocellular carcinoma. Int. J. Oncol. **26**:673–678.
59. **Tannenbaum GS, Choi HK, Gurd W, Waxman DJ.** 2001. Temporal relationship between the sexually dimorphic spontaneous GH secretory profiles and hepatic STAT5 activity. Endocrinology **142**:4599–4606.
60. **Vidal OM, et al.** 2007. In vivo transcript profiling and phylogenetic analysis identifies suppressor of cytokine signaling 2 as a direct signal transducer and activator of transcription 5b target in liver. Mol. Endocrinol. **21**:293–311.
61. **Wauthier V, Sugathan A, Meyer RD, Dombkowski AA, Waxman DJ.** 2010. Intrinsic sex differences in the early growth hormone responsiveness of sex-specific genes in mouse liver. Mol. Endocrinol. **24**:667–678.
62. **Wauthier V, Waxman DJ.** 2008. Sex-specific early growth hormone response genes in rat liver. Mol. Endocrinol. **22**:1962–1974.
63. **Waxman DJ, Holloway MG.** 2009. Sex differences in the expression of hepatic drug metabolizing enzymes. Mol. Pharmacol. **76**:215–228.
64. **Waxman DJ, Pampori NA, Ram PA, Agrawal AK, Shapiro BH.** 1991. Interpulse interval in circulating growth hormone patterns regulates sexually dimorphic expression of hepatic cytochrome P450. Proc. Natl. Acad. Sci. U. S. A. **88**:6868–6872.
65. **Waxman DJ, Ram PA, Park SH, Choi HK.** 1995. Intermittent plasma growth hormone triggers tyrosine phosphorylation and nuclear translocation of a liver-expressed, Stat 5-related DNA binding protein. Proposed role as an intracellular regulator of male-specific liver gene transcription. J. Biol. Chem. **270**:13262–13270.
66. **Xu J, et al.** 2011. Exploring endocrine GH pattern in mice using rank plot analysis and random blood samples. J. Endocrinol. **208**:119–129.
67. **Yang X, et al.** 2006. Tissue-specific expression and regulation of sexually dimorphic genes in mice. Genome Res. **16**:995–1004.
68. **Zanger UM, Turpeinen M, Klein K, Schwab M.** 2008. Functional pharmacogenetics/genomics of human cytochromes P450 involved in drug biotransformation. Anal. Bioanal Chem. **392**:1093–1108.
69. **Zhang Y, et al.** 2011. Transcriptional profiling of human liver identifies sex-biased genes associated with polygenic dyslipidemia and coronary artery disease. PLoS One **6**:e23506.
70. **Zhang Y, et al.** 2008. Model-based analysis of ChIP-Seq (MACS). Genome Biol. **9**:R137.
71. **Zhou YC, Waxman DJ.** 1999. STAT5b down-regulates peroxisome proliferator-activated receptor alpha transcription by inhibition of ligand-independent activation function region-1 trans-activation domain. J. Biol. Chem. **274**:29874–29882.